



UNIVERSIDADE FEDERAL DO PARÁ
INSTITUTO DE GEOCIÊNCIAS
PROGRAMA DE PÓS-GRADUAÇÃO EM GEOFÍSICA

DISSERTAÇÃO DE MESTRADO

**A study on 1D joint and laterally constrained inversion
of 2D EMMF, CSAMT and MT data using analytical
derivatives**

DANIELA COSTA MELO

Belém-PA
2019

DANIELA COSTA MELO

**A study on 1D joint and laterally constrained inversion
of 2D EMMF, CSAMT and MT data using analytical
derivatives**

Dissertação apresentada ao Programa de Pós-Graduação
em Geofísica do Instituto de Geociências da Universi-
dade Federal do Pará para obtenção do título de Mestre
em Geofísica.

Área de concentração:
Modelagem e inversão de dados geofísicos

Linha de pesquisa:
Incorporação de vínculos no problema geofísico inverso

Orientador: Prof. Dr. Cícero Roberto Teixeira Régis

Belém-PA
2019

**Dados Internacionais de Catalogação na Publicação (CIP) de acordo com ISBD
Sistema de Bibliotecas da Universidade Federal do Pará
Gerada automaticamente pelo módulo Ficat, mediante os dados fornecidos pelo(a) autor(a)**

M528s

Melo, Daniela Costa.

A study on 1D joint and laterally constrained inversion of 2D EMMF, CSAMT and MT data using analytical derivatives / Daniela Costa Melo. — 2019.
49 f. : il. color.

Orientador(a): Prof. Dr. Cícero Roberto Teixeira Régis

Dissertação (Mestrado) - Programa de Pós-Graduação Geofísica, Instituto de Geociências, Universidade Federal do Pará, Belém, 2019.

1. Inversão conjunta. Inversão lateralmente vinculada (LCI). Métodos eletromagnéticos. I. Título.

CDD 622.15

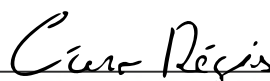
DANIELA COSTA MELO

**A study on 1D joint and laterally constrained inversion of 2D
EMMF, CSAMT and MT data using analytical derivatives**

Dissertação apresentada ao Programa de Pós-Graduação
em Geofísica do Instituto de Geociências da Universi-
dade Federal do Pará para obtenção do título de Mestre
em Geofísica.

Data de aprovação: 1º de abril de 2019

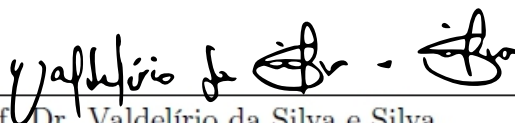
Banca Examinadora:



Prof. Dr. Cícero Roberto Teixeira Régis (Orientador)
Universidade Federal do Pará



Profa. Dra. Aline Tavares Melo
Universidade Federal de Minas Gerais



Prof. Dr. Valdelírio da Silva e Silva
Universidade Federal do Pará

I dedicate this work to my husband who, by believing in me, did not let me give up and is constantly helping me to continue pursuing my goals.

AGRADECIMENTOS

I thank all my professors at UFPA, specially my advisor Prof. Dr. Cícero Régis who helped not only with advices and ideias to develop this work but also with encouragement.

I also thank all my colleagues at CPGf-UFPA, from services staff to PROEM partners. To my colleague Jarol David Garcia Perez for providing the 2D modeling codes for both the circular loop and horizontal electric dipole. To Érico Tenório França for helping me with the analytical derivatives calculation.

To CNPQ for providing the financial support for the development of this work. Moreover, I would like to thank all the other sponsors I had through my academic life, namely PET-MEC, CAPES-Brazilian Science Without Borders, Petrobras and INCT-GP.

Lastly, to my family and husband for all the encouragement, support and friendship.

RESUMO

Embora as inversões convencionais de dados separados possam gerar modelos úteis, resultados melhores podem ser obtidos através de inversão conjunta uma vez que essa informação extra adicionada reduz a ambiguidade ou a não-unicidade do problema. Foi avaliado um esquema de inversão conjunta aplicado a três diferentes métodos eletromagnéticos: Audiomagnetotelúrico de Fonte Controlada (CSAMT), Método Eletromagnético a Multi-frequência (EMMF) e Magnetotelúrico (MT). Estes múltiplos conjuntos de dados são combinados e invertidos dois a dois, a fim de estimar um modelo comum de parâmetros (condutividades) que ajustam simultaneamente ambos os conjuntos de dados. Utilizamos uma técnica de inversão com vínculos na lateral para estimar modelos pseudo-2D e aplicamos o método de Marquardt para resolver os problemas de inversão conjunta 1D, regularizados com Suavidade Global ou Variação Total. Exemplos com dados sintéticos 1D e 2D demonstraram que os modelos derivados da inversão conjunta dos métodos EMMF+CSAMT e CSAMT+MT resolvem melhor as variações de resistividade da subsuperfície terrestre já que esses métodos fornecem informações complementares.

Palavras-chaves: Inversão conjunta. Inversão lateralmente vinculada (LCI). Métodos eletromagnéticos.

ABSTRACT

Although conventional separate inversions can generate useful models, better results can be derived from jointly estimated models since this extra information reduces the ambiguity or non-uniqueness of the problem. We evaluated a joint inversion scheme applied to three different EM methods: Controlled Source Audio-Magnetotelluric (CSAMT), Multi-frequency Electromagnetic Method (EMMF) and Magnetotelluric (MT). These multiple data sets are combined and inverted two by two in order to estimate a common parameters model (conductivities) that simultaneously fit both measurement sets. We use a laterally constrained inversion (LCI) technique to estimate pseudo-2D models and apply the Marquardt's method to solve the 1D joint inverse problems, regularized with either Global Smoothness or Total Variation. Examples with synthetic 1D and 2D data demonstrates that models derived from joint EMMF+CSAMT and CSAMT+MT inversion better resolve the Earth's subsurface resistivity variations as these methods provide complementary information.

Keywords: Joint inversion. Laterally constrained inversion (LCI). Electromagnetic methods.

LIST OF FIGURES

2.1	Vertical and lateral constraints in 1D structures positioned side by side. The red triangles are measuring stations.	3
2.2	Acquisition geometry.	4
3.1	Model of N homogeneous and isotropic horizontal layers.	5
4.1	Vertical and lateral constraints in a 3-layer model with two adjacent soundings. The red triangles are measuring stations.	14
4.2	Sensitivities calculated for the EMMF, CSAMT and MT observations. Each column corresponds to the sensitivity of a layered medium at a specific frequency. The vertical axis is the depth of the interpretative model interfaces.	19
5.1	1D Model used to generate the 1D synthetic data. The field measurements were taken at $x = 7$ km.	20
5.2	Final 1D models obtained by isolated and joint inversion of the EMMF, CSAMT and MT methods using the Global Smoothness regularization. The conductivities of each layer start as an initial guess represented by the dashed red lines and their estimated values (after the inversion) are shown by the black lines in “stairs” format.	21
5.3	Final 1D models obtained by isolated and joint inversion of the EMMF, CSAMT and MT methods using the Total Variation regularization.	21
5.4	Final 1D models obtained by isolated and joint inversion of the EMMF, CSAMT and MT methods using the Global Smoothness regularization.	23
5.5	Final 1D models obtained by isolated and joint inversion of the EMMF, CSAMT and MT methods using the Total Variation regularization.	23
6.1	2D Model. The field measurements were taken along a 5 km survey line at the surface, starting at $x = 4500$ m with a receiver spacing of 200 m.	25
6.2	EMMF, CSAMT and MT synthetic observed data generated from Model 1.	26
6.3	Final pseudo-2D models obtained by isolated and joint inversion of the EMMF, CSAMT and MT methods using the Global Smoothness regularization.	27
6.4	Final pseudo-2D models obtained by isolated and joint inversion of the EMMF, CSAMT and MT methods using the Total Variation regularization.	27
6.5	EMMF, CSAMT and MT synthetic observed data generated from Model 2.	29

6.6	Final pseudo-2D models obtained by isolated and joint inversion of the EMMF, CSAMT and MT methods using the Global Smoothness regularization.	30
6.7	Final pseudo-2D models obtained by isolated and joint inversion of the EMMF, CSAMT and MT methods using the Total Variation regularization.	30
6.8	2D Model.	32
6.9	EMMF, CSAMT and MT synthetic observed data generated from Model 3.	32
6.10	Final pseudo-2D models obtained by isolated and joint inversion of the EMMF, CSAMT and MT methods using the Global Smoothness regularization.	33
6.11	Final pseudo-2D models obtained by isolated and joint inversion of the EMMF, CSAMT and MT methods using the Total Variation regularization.	33

SUMMARY

1	INTRODUCTION	1
2	METHODOLOGY	3
3	FORWARD PROBLEMS	5
3.1	EMMF	6
3.2	CSAMT	8
3.3	MT	10
4	INVERSE PROBLEM	11
4.1	REGULARIZED INVERSE PROBLEM	11
4.1.1	Global Smoothness	12
4.1.2	Total Variation	12
4.1.3	Matrix S	13
4.2	GAUSS-NEWTON METHOD WITH MARQUARDT'S STRATEGY . .	15
4.3	ANALYTICAL DERIVATIVES	16
4.3.1	EMMF	17
4.3.2	CSAMT	17
4.3.3	MT	19
5	1D INVERSION RESULTS	20
5.1	MODEL 1	20
5.2	MODEL 2	22
6	LCI RESULTS	25
6.1	MODEL 1	25
6.2	MODEL 2	28
6.3	MODEL 3	31
7	CONCLUSIONS	35
	REFERENCES	36

1 INTRODUCTION

Inversion of geophysical data can generate useful models of the underlying anomalies hence facilitating the geological interpretation. However, the geophysical inversion problem is intrinsically ill-posed in the sense that a number of different models can explain the data (ambiguity). Additionally, in most cases, inversion problems are underdetermined and the data are affected by noise, which increases the ambiguity of the inversion. To reduce this problem, a regularization factor is introduced into the objective function. Furthermore, data acquired with different geophysical methods are typically affected by different interference sources; therefore, the joint inversion of multiple geophysical data can not only mitigate the noise, but also reduce the ambiguity or non-uniqueness of the problem.

Joint inversion was first proposed by Vozoff and Jupp (1975). Subsequently, Sasaki (1989) presented a two-dimensional joint inversion of magnetotelluric (MT) and dipole–dipole resistivity data to recover the distribution of underground resistivity. The example of 1D joint marine controlled-source electromagnetic method (MCSEM) and marine MT (MMT) inversion shown in Constable and Weiss (2006) present improvement of the resolution of a thin resistor relative to the MCSEM-only case. Similarly, Mackie et al. (2007) extend this problem to the 3D inversion case. Then Abubakar et al. (2011) propose a multiplicative cost function instead of the traditional additive one in order to address the weighting problem and adaptively put CSEM and MT data on equal footing in the inversion process. Auken et al. (2007) show that the resolution of the subsurface resistivity structures is significantly enhanced if transient electromagnetic (TEM) x- and z-component data are inverted jointly. Candansayar and Tezkan (2008) could resolve both near-surface and deeper structure by using a 2D joint inversion of radiomagnetotelluric (RMT) and DC resistivity data. Jegen et al. (2009) presented excellent results using his joint inversion applied to marine exploration data.

The methods tested in this work were MT, CSAMT and EMMF. The first method lies on the MT fields nature which are basically plane-waves and horizontally uniform over large distances. Its source are naturally occurring signals, enabling investigation from many tens to hundreds of kilometers and because of that, it is routinely used to image regional electrical resistivity structures. The Controlled Source Audio-Magnetotellurics (CSAMT) is a method derived from MT, with the main difference that it uses an artificial EM source (typically grounded electric dipole) in the range 0.1 Hz to 10 kHz, so its high frequency content is responsible for addressing near surface targets. Many different works have been published to show that the method can contribute to better determination of near surface electrical distributions (Ismail et al., 2011; Pedrera et al., 2016). Along with those, there are some papers on CSAMT inversion, for instance Mitsuhashi et al. (2002)

developed an algorithm to invert frequency-domain vertical magnetic data generated by a grounded-wire source for a 2D model of the earth (2.5-D inversion); Lei et al. (2010) shows a study on 2D CSAMT modelling and inversion taking into account source and topography effects. More recently, Lin et al. (2018) presented 3D inversion results along with a scheme to incorporate topographic distortions into the inversion instead of correcting them.

The other electromagnetic method used in this work was the new Multi-frequency electromagnetic method (EMMF) which basically has the purpose of inductively measuring the ground electrical resistivity and induced polarization (IP). Although it has its origins back to 1968 (Dias, 1968), only very recently it has been receiving contributions in terms of improved equipment design, theoretical and field work, specific software development for data processing and interpretation procedures (Dias, 2000; Dias et al., 2012, 2006, 2005; Machado, 2009; Machado and Dias, 2012; Sifontes et al., 2016). A few studies have been published on inversion of EMMF data (Piedade and Régis, 2014; Piedade et al., 2015).

To invert the data, in this work we apply an efficient and fast inversion algorithm that uses a 1D joint and laterally constrained inversion (LCI) of data from the whole set of sounding stations on a survey line. Data from CSAMT, EMMF and MT methods are combined two by two and inverted jointly. Miorelli (2011) has successfully applied a similar algorithm, showing good consistency with the 1D LCI inversion results obtained from 3D data. These inversion algorithms are an implementation of a 1D laterally constrained inversion technique (Santos, 2004; Auken and Christiansen, 2004; Auken et al., 2005) using analytical derivatives to build the Jacobian matrix and, specifically in this work, we have also applied two different regularizations methods: Global Smoothness (Constable et al., 1987) and Total Variation (Martins et al., 2011). The biggest advantage of LCI techniques is its capacity of performing inversion of large datasets at a low computational cost. An analysis of the joint inversion methodology is performed for (i) 1D inversion of data generated by two different 1D models and (ii) 1D LCI of three synthetic data sets generated from 2D models.

2 METHODOLOGY

The study was done by analyzing (i) 1D inversion results with regularizations in the vertical direction only and (ii) results from a pseudo-2D technique that uses 1D forward modeling and lateral constraints (laterally constrained inversion - LCI).

This LCI method performs joint inversion of data from a set of sounding stations by including all the data in a single cost function. Each observation is associated with a layered model beneath its location, each one generating a 1D sequence of conductivity values that represent a vertical column. The final 2D model is built by a lateral collation of 1D layered models, applying lateral constraints between adjacent conductivities (Fig. 2.1). Detailed information on how to apply both vertical and lateral constraints will be given in “Matrix S” subsection (4.1.3) in chapter 4.

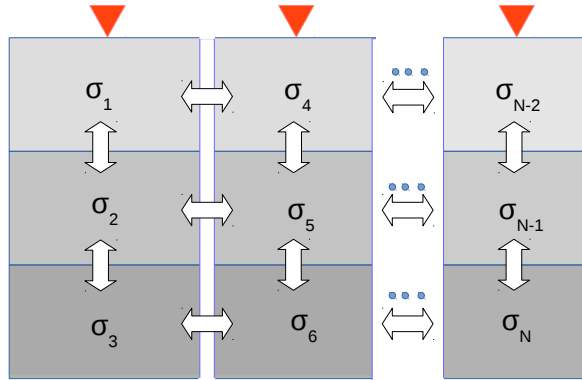


Figure 2.1: Vertical and lateral constraints in 1D structures positioned side by side. The red triangles are measuring stations.

In this study, the 2D observed data \mathbf{d} are the real and imaginary components of the radial magnetic (\mathbf{H}_r) and electric fields (\mathbf{E}_x) for the EMMF and CSAMT methods, respectively, and the real and imaginary components of the surface apparent impedance ($\hat{\mathbf{Z}}_1$) from transverse magnetic (TM) propagation mode in the MT case. In such scenarios, magnetic and electric field measurements are taken over the x axis. For the EMMF method, we consider a circular loop as its source and, specifically for the CSAMT case, we consider a horizontal electrical dipole located in the x direction (Fig. 2.2).

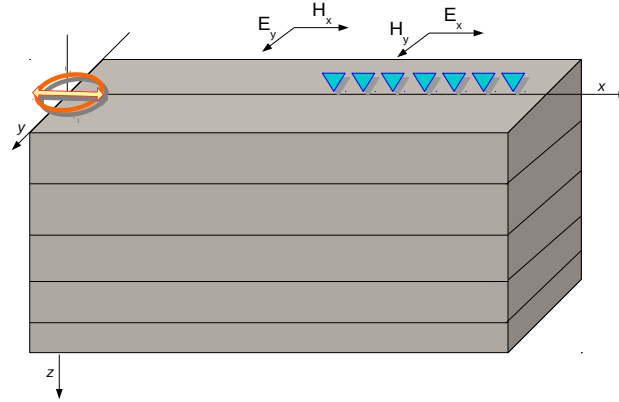


Figure 2.2: Acquisition geometry.

The interpretative model is a horizontal plane-parallel layered medium (Fig. 3.1) for each sounding and the parameters are the logarithmic values of the conductivities of each layer (logarithms are used to avoid negative conductivities). This model is the one for which the conductivities will be estimated by the inversion, hence it receives this name (interpretative) because it is the physical model that will be used to help the geological interpretation.

3 FORWARD PROBLEMS

The forward problem consists on numerical modeling of data from a given set of parameters (model). In geophysics, the parameters are values of a certain physical property of the subsurface of the Earth and the solution of the forward problem makes it possible to predict the geophysical data for certain geological structures.

In this study, the three forward problems consist in simulating the data set generated by a 1D layered Earth's subsurface. It is formed at the top by an isotropic and infinite homogeneous half-space representing the air ($\sigma_0 = 10^{-12}S/m$), and just below another semi-space formed by N parallel layers, also homogeneous of finite thickness h_j , ending in another infinite semi-space: the substrate. In this model, the substrate is the last layer (N -th layer) and has infinite thickness. See Figure 3.1.

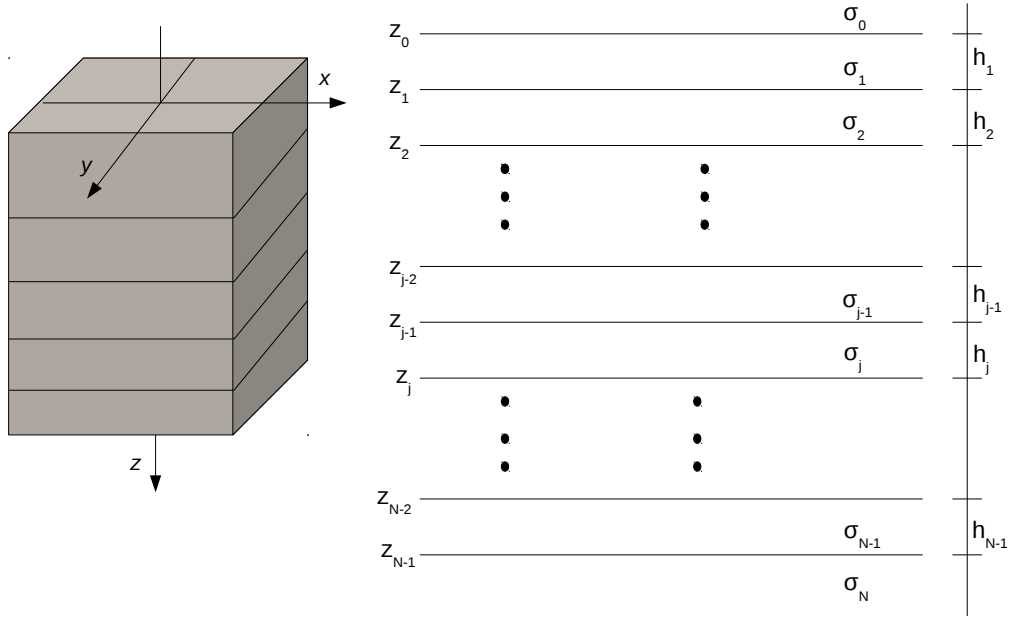


Figure 3.1: Model of N homogeneous and isotropic horizontal layers.

To determine the fields produced by this layered medium, one must start with Maxwell's equations in the frequency domain:

$$\nabla \cdot \epsilon \mathbf{E} = 0 \quad (3.1)$$

$$\nabla \times \mathbf{E} + \zeta \mathbf{H} = 0 \quad (3.2)$$

$$\nabla \cdot \mu \mathbf{B} = 0 \quad (3.3)$$

$$\nabla \times \mathbf{H} - \eta \mathbf{E} = \mathbf{J}_S \quad (3.4)$$

where \mathbf{E} and \mathbf{H} are the electric and magnetic fields, \mathbf{J}_S is the current density, $\eta = \sigma + i\omega\epsilon$

and $\zeta = i\omega\mu$ ($i = \sqrt{-1}$). The quantities ω , ϵ and μ are the angular frequency, electric permittivity (F/m) and magnetic permeability (H/m), respectively.

3.1 EMMF

A horizontal square loop with its sides measuring hundreds of meters and extended to the ground surface ($h_0 = 0$) is used as the EMMF's source. It operates using several frequencies and the response of the radial horizontal magnetic field $\mathbf{H}_r(r, z)$, produced by inductive effects, is collected at vertical loop receiving coils (also located at the surface). Detailed information about the method can be found in Dias et al. (2019), Silva (2012) and Piedade (2014).

Machado (2009) demonstrates that for the source-receiver offsets used in the method's surveys, the square source can be approximated by and modeled as a horizontal circular loop. The current density \mathbf{J}_S for a loop with current $I(\omega)$, frequency ω dependent, radius a and located at a height of h_0 is given by:

$$\mathbf{J}_S = I(\omega) \frac{a}{r} \delta(r - a) \delta(z - h_0) \hat{\phi} \quad (3.5)$$

Combining equations 3.2, 3.4 and 3.5, it is possible to write a second order equation in cylindrical coordinates:

$$\left(\frac{\partial^2 E_\phi}{\partial r^2} + \frac{1}{r} \frac{\partial E_\phi}{\partial r} - \frac{E_\phi}{r^2} \right) + \frac{\partial^2 E_\phi}{\partial z^2} + k^2 E_\phi = \zeta I(\omega) \frac{a}{r} \delta(r - a) \delta(z - h_0) \quad (3.6)$$

where $k^2 = -\eta\zeta$ is the wavenumber.

$$\mathcal{H}_v \left[\frac{\partial^2 f(r)}{\partial r^2} + \frac{1}{r} \frac{\partial f(r)}{\partial r} - \frac{v^2}{r^2} f(r) \right] = -k_r^2 \hat{f}(k_r) \quad (3.7)$$

$$\mathcal{H}_v \left[\frac{\delta(r - a)}{r} \right] = J_v(k_r a) \quad (3.8)$$

If a first order ($v=1$) Hankel transform (Abramowitz and Stegun, 1964) is applied in equation 3.6 and using the identities provided in 3.7 and 3.8, equation 3.9 is obtained:

$$\frac{\partial^2 \hat{E}_\phi}{\partial z^2} - u^2 \hat{E}_\phi = \zeta I(\omega) a J_1(k_r a) \delta(z - h_0) \quad (3.9)$$

with $u^2 = k_r^2 - k^2$. The solution for this equation is

$$\hat{E}_\phi(k_r, z) = -\zeta I(\omega) a J_1(k_r a) \frac{e^{-u|z-h_0|}}{2u} \quad (3.10)$$

which is an equation that describes $\hat{E}_\phi(k_r, z)$ as a plane-wave field in the (k_r, z) domain.

For a horizontal layered medium and supposing measurements are taken at the surface level, equation 3.11 turns into equation 3.12 since $j = 0$ and $h_0 = 0$.

$$\hat{E}_\phi^{(j)}(k_r, z) = E_j(e^{-u_j(z-z_{j-1})} + R_{TE}^j e^{u_j(z-z_j)}) \quad (3.11)$$

$$\hat{E}_\phi^{(0)}(k_r, z) = E_0(1 + R_{TE}^{(0)}) \quad (3.12)$$

where E_0 and $R_{TE}^{(0)}$ are the transmission and reflexion coefficients, respectively, at the surface level. The former is given by equation 3.13 and the latter can be obtained by 3.14.

$$E_0 = \frac{-\zeta_0 I(\omega) a J_1(k_r a) e^{u_0 h_0}}{2u_0} \quad (3.13)$$

$$R_{TE}^{(0)} = \frac{\chi_0 - \hat{\chi}_1}{\chi_0 + \hat{\chi}_1} \quad (3.14)$$

with $\hat{\chi}_1$ representing the surface apparent admittance, which is calculated using the recursive formula bellow:

$$\hat{\chi}_j = \chi_j \frac{\hat{\chi}_{j+1} + \chi_j \tanh(u_j h_j)}{\chi_j + \hat{\chi}_{j+1} \tanh(u_j h_j)}, j = N - 1, \dots, 2, 1 \quad (3.15)$$

$$\hat{\chi}_N = \chi_N \quad (3.16)$$

with

$$\chi_j = \frac{u_j}{\zeta_j} = \frac{\sqrt{k_r^2 - k_j^2}}{\zeta_j} \quad (3.17)$$

Substituting equation 3.11 in 3.2, we can determine the radial horizontal magnetic field in the $/k_r, z/$ domain:

$$\hat{H}_r^{(j)}(k_r, z) = -\chi_j E_j (e^{-u_j(z-z_{j-1})} - R_{TE}^j e^{u_j(z-z_j-h_j)}) \quad (3.18)$$

and by applying an inverse Hankel transform, we have the same response but now in the spatial (r, z) domain.

$$H_r^{(j)}(r, z) = \int_0^\infty \hat{H}_r^{(j)}(k_r, z) J_1(k_r r) k_r dk_r \quad (3.19)$$

Since we are collecting the responses at surface level ($z = 0$), then

$$H_r^{(0)}(r, z) = \int_0^\infty -\chi_0 E_0 (1 - R_{TE}^{(0)}) J_1(k_r r) k_r dk_r \quad (3.20)$$

The integral transform in 3.20 does not have a known analytical solution, thus it needs to be numerically evaluated with the use of digital filters to solve it (Werthmüller et al.,

2019). The observations are the real and imaginary components of the radial horizontal magnetic field $H_r(r, \omega)$ normalized by the vertical component of a magnetic dipole $H_z^0(r)$ of magnetic moment m , located in the vacuum (Ward et al., 1987):

$$\bar{H} = \frac{H_r(r, \omega)}{H_z^0(r)} \quad (3.21)$$

where

$$H_z^0(r) = \frac{-m}{4\pi r^3} \quad (3.22)$$

This normalization dampers the geometric decrease in field intensity with increasing distance from the source, emphasizing the conductivity variations in the medium.

3.2 CSAMT

The CSAMT source is usually a horizontal electrical dipole measuring between 1 km and 2 km of length. Each sounding station is located about four times the skin-depth¹ from the transmitter (Zonge and Hughes, 1991). Receivers record both the electric field, parallel to the grounded wire, and the magnetic field, perpendicular to the grounded wire. Electrical and magnetic fields are measured by electrodes and antennas, respectively. More details can be found in Perez (2016).

In equation 3.4, the term \mathbf{J}_S is the CSAMT source. The source used to calculate the 1D forward responses is x-directed and located in (x_0, y_0, h_0) , its expression is:

$$\mathbf{J}_S = I(\omega) dS_x \delta(x - x_0) \delta(y - y_0) \delta(z - h_0) \hat{e}_x \quad (3.23)$$

For this type of source the TE (electric transverse) and TM (magnetic transverse) propagation modes exist simultaneously. Thus, the electromagnetic fields will be given by the sum of these two modes of propagation. The general expressions for the electric and magnetic fields, in terms of the Schelkunoff potentials approach (Ward et al., 1987) are:

$$\mathbf{E} = -\nabla \times \mathbf{F} - \zeta \mathbf{A} + \frac{1}{\eta} \nabla(\nabla \cdot \mathbf{A}) \quad (3.24)$$

$$\mathbf{H} = \nabla \times \mathbf{A} - \eta \mathbf{F} + \frac{1}{\zeta} \nabla(\nabla \cdot \mathbf{F}) \quad (3.25)$$

For the particular case in which the potential \mathbf{F} is zero and the potential \mathbf{A} has only the z-component A_z , only electromagnetic fields of TM mode, with respect to the z direction, are generated. On the other hand, if the potential \mathbf{A} is zero and the potential \mathbf{F} has only the z-component F_z , fields in the TE mode are generated, also in respect to the z-direction.

¹The skin-depth provides a quantitative measure of how the field attenuates as it propagates through the conductive medium. Its mathematical formula is: $\frac{500}{\pi} \sqrt{\frac{10}{f\sigma}}$

The total fields are a composition of these two particular cases, their components are:

$$E_x = \frac{1}{\eta} \frac{\partial^2 A_z}{\partial x \partial z} - \frac{\partial F_z}{\partial y} \quad (3.26)$$

$$E_y = \frac{1}{\eta} \frac{\partial^2 A_z}{\partial y \partial z} + \frac{\partial F_z}{\partial x} \quad (3.27)$$

$$E_z = \frac{1}{\eta} \left(\frac{\partial^2}{\partial z^2} + k^2 \right) A_z \quad (3.28)$$

$$H_x = \frac{1}{\zeta} \frac{\partial^2 F_z}{\partial x \partial z} + \frac{\partial A_z}{\partial y} \quad (3.29)$$

$$H_y = \frac{1}{\zeta} \frac{\partial^2 F_z}{\partial y \partial z} - \frac{\partial A_z}{\partial x} \quad (3.30)$$

$$H_z = \frac{1}{\zeta} \left(\frac{\partial^2}{\partial z^2} + k^2 \right) F_z \quad (3.31)$$

By performing an analysis similar to that performed by Farias (2012) to obtain F_z and A_z , we can determine the final expression for the components of the electromagnetic field in the space domain (x, y, z) as a function of the electric dipole moment $I(\omega)dS_x$. The expression for the component we are interested in is:

$$\begin{aligned} E_x^{(0)}(r, \omega) = & -\frac{IdS_x}{4\pi} \left(\frac{1}{r} - \frac{2x^2}{r^3} \right) \int_0^\infty (1 - R_{TM}^{(0)}) Z_0 J_1(k_r r) dk_r \\ & - \frac{IdS_x}{4\pi} \frac{x^2}{r^2} \int_0^\infty (1 - R_{TM}^{(0)}) Z_0 J_0(k_r r) k_r dk_r \\ & - \frac{IdS_x}{4\pi} \left(\frac{1}{r} - \frac{2y^2}{r^3} \right) \int_0^\infty (1 + R_{TE}^{(0)}) \frac{1}{\chi_0} J_1(k_r r) dk_r \\ & - \frac{IdS_x}{4\pi} \frac{y^2}{r^2} \int_0^\infty (1 + R_{TE}^{(0)}) \frac{1}{\chi_0} J_0(k_r r) k_r dk_r \end{aligned} \quad (3.32)$$

$R_{TM}^{(0)}$ and $R_{TE}^{(0)}$ are the reflection coefficients for the TM and TE propagation modes, respectively, at the surface. The latter is given by 3.14 and the former, by the following expression:

$$R_{TM}^{(0)} = \frac{Z_0 - \hat{Z}_1}{Z_0 + \hat{Z}_1} \quad (3.33)$$

with \hat{Z}_1 representing the surface apparent impedance, which is calculated using the recursive formula bellow:

$$\hat{Z}_j = Z_j \frac{\hat{Z}_{j+1} + Z_j \tanh(u_j h_j)}{Z_j + \hat{Z}_{j+1} \tanh(u_j h_j)}, j = N - 1, \dots, 2, 1 \quad (3.34)$$

$$\hat{Z}_N = Z_N \quad (3.35)$$

with

$$Z_j = \frac{u_j}{\eta_j} = \frac{\sqrt{k_r^2 - k_j^2}}{\eta_j} \quad (3.36)$$

As in the EMMF case, the integral transform in 3.32 does not have a known analytical solution, thus we used digital filters (Werthmüller et al., 2019) to solve for E_x . The observations are the real and imaginary components of the radial electrical field $E_x(r, \omega)$ normalized by its dipole moment $p = I(\omega)dS_x$ and a factor to correct the geometric damping:

$$\bar{E} = \frac{E_x(r, \omega)}{E'(r)} \quad (3.37)$$

where

$$E'(r) = \frac{p}{\pi r^3} \quad (3.38)$$

3.3 MT

The MT assumption is a vertically incident plane-wave caused by natural variations in the Earth's magnetosphere, which induces horizontal electric currents (known as telluric currents) in the subsurface. Given the electrical conductivities σ_j and thicknesses h_j of each layer, it is possible to determine the components of the apparent impedance tensor at the surface \hat{Z}_1 using equation 3.34. Additionally, apparent resistivity ρ_a and phase ϕ , both depending on frequency ω , can be calculated using the equations below (Vozoff, 1991):

$$\rho_a = \frac{1}{\omega\mu_0} |\hat{Z}_1|^2 \quad (3.39)$$

$$\phi = \tan^{-1} \left[\frac{\text{Im}(\hat{Z}_1)}{\text{Re}(\hat{Z}_1)} \right] \quad (3.40)$$

where μ_0 is the magnetic permeability of the vacuum. The apparent resistivity ρ_a corresponds to the resistivity of a half-space equivalent to the stratified medium.

4 INVERSE PROBLEM

Most of the geophysical problems are non-linear, meaning that the observed data are not a linear combination of the model parameters. A geophysical dataset \mathbf{d} , with N_o observations, is to be fit by synthetic data generated from the N_p model parameters in vector \mathbf{P} . The relationship between the synthetic data (for each method) and the parameter set is in the form

$$\mathbf{d}^{\text{EMMF}} = \mathbf{F}^{\text{EMMF}}(\mathbf{P}), \quad (4.1)$$

$$\mathbf{d}^{\text{CSAMT}} = \mathbf{F}^{\text{CSAMT}}(\mathbf{P}), \quad (4.2)$$

$$\mathbf{d}^{\text{MT}} = \mathbf{F}^{\text{MT}}(\mathbf{P}), \quad (4.3)$$

where \mathbf{F} is a non-linear vector function that represents the forward modeling operator. This vector function also depends on the frequency ω , and on the measurement position (x, y, z) .

Since the function \mathbf{F} doesn't have a unique inverse, the problem of determining a set of parameters that generate synthetic data that approximate the observations is defined as that of minimizing a functional ϕ_d that measures the misfit of the model's forward response $\mathbf{F}(\mathbf{P})$ for a given set of parameters \mathbf{P} to the observed data \mathbf{d} :

$$\phi_d(\mathbf{P}) = \|\mathbf{d} - \mathbf{F}(\mathbf{P})\|^2 = [\mathbf{d} - \mathbf{F}(\mathbf{P})]^T [\mathbf{d} - \mathbf{F}(\mathbf{P})] \quad (4.4)$$

in the joint approach used in this study,

$$\phi_d = \phi_{\text{EMMF}} + \phi_{\text{CSAMT}} \quad \text{or} \quad (4.5)$$

$$\phi_d = \phi_{\text{CSAMT}} + \phi_{\text{MT}} \quad \text{or} \quad (4.6)$$

$$\phi_d = \phi_{\text{EMMF}} + \phi_{\text{MT}} \quad (4.7)$$

Optimization methods are used to find the solution of this type of problem, where the objective is to find the minimum of the data misfit functional ϕ_d , that is, to minimize the difference between observed data and calculated data. In this study, the minimization of the nonlinear functional ϕ_d , with respect to \mathbf{P} , was performed iteratively by the Gauss-Newton method with the Marquardt's modification (Marquardt, 1963; Pujol, 2007).

4.1 REGULARIZED INVERSE PROBLEM

In geophysical applications, there is an infinite number of solutions that explain geophysical observations within experimental accuracy. One way of making this problem

well-posed, is to introduce a priori information about the parameters to be estimated. This is done by including regularizing functionals ϕ_{REG} defined from a desired relationship between parameters, and acting not only as mathematical devices to stabilize the inverse geophysical problem, but also as constraints that reflect the geological and physical characteristics of the Earth's different environments.

After the introduction of regularization, the solutions to the inversion problem are obtained from the minimization of both ϕ_d and ϕ_{REG} as parts of a single function called objective function ϕ_α :

$$\phi_\alpha(\mathbf{P}) = \phi_d(\mathbf{P}) + \alpha \phi_{REG}(\mathbf{P}), \quad (4.8)$$

where α is a positive scalar, called the regularization parameter, which controls the relative weight of the information introduced by the regularizing functional to the inversion process.

In this work two regularization functions were used: Global Smoothness ϕ_{GS} and Total Variation ϕ_{TV} .

4.1.1 Global Smoothness

The Global Smoothness or first-order Tikhonov regularization (Tikhonov and Arsenin, 1977) is the well-known Occam's inversion (Constable et al., 1987) that leads to solutions in which the differences between parameter values are minimal, that is, variations between parameter values are smooth. The mathematical representation of the functional ϕ_{GS} is:

$$\phi_{GS}(\mathbf{P}) = \|\mathbf{S}\mathbf{P}\|_2^2, \quad (4.9)$$

where \mathbf{S} is a matrix which stores the constraints between the parameters. More details about how this matrix is organized can be found in the "Matrix S" subsection (4.1.3).

The gradient vector \mathbf{g}^{GS} and the Hessian matrix \mathbf{H}^{GS} of ϕ_{GS} are, respectively:

$$\mathbf{g}^{GS} = \nabla_p \phi_{GS}(\mathbf{P}) = 2\mathbf{S}^t \mathbf{S} \mathbf{P}, \quad (4.10)$$

$$\mathbf{H}^{GS} = \nabla_p \nabla_p^t \phi_{GS}(\mathbf{P}) = 2\mathbf{S}^t \mathbf{S} \quad (4.11)$$

By minimizing the functional ϕ_α (Eq. 4.8) with the global smoothness regularization, solutions are the parameters corresponding to the smoothest model that fits the data.

4.1.2 Total Variation

Smooth models representative of the subsurface geological structures are not always desirable. There are cases where sharp discontinuities in the resistivity, as in faults or intrusions, should be allowed in the models. The global smoothness regularization leads to solutions in which regions of discontinuities are detected, but softened in the solution

model. On the other hand, the Total Variation regularizer does not penalize sharp variations, clearly marking the abrupt changes in the parameter values. The mathematical representation of the functional ϕ_{TV} is (Martins et al., 2011):

$$\phi_{TV}(P) = \sum_{i=1}^{N_d-1} |(P_{i+1} - P_i)|, \quad (4.12)$$

or in matrix form

$$\phi_{TV}(\mathbf{P}) = \|\mathbf{S}\mathbf{P}\|_1. \quad (4.13)$$

where \mathbf{S} is a matrix which stores the constraints between the parameters (see subsection 4.1.3) and $\|\cdot\|_1$ is the l_1 norm² of the vector of differences between parameters.

However, if $P_{i+1} = P_i$, the functional ϕ_{TV} is not differentiable. To overcome this problem, Vogel (1997) proposed the approximation:

$$\phi_{TV}(P) \cong \sum_{k=1}^{N_d} [(P_i - P_j)_k^2 + \beta]^{1/2}, \quad (4.14)$$

where β is a small and positive scalar.

The gradient vector and the Hessian of ϕ_{TV} are, respectively:

$$\mathbf{g}^{TV} = \mathbf{S}^T \mathbf{q}, \quad (4.15)$$

$$\mathbf{H}^{TV} = \mathbf{S}^T \mathbf{Q} \mathbf{S}, \quad (4.16)$$

where \mathbf{q} is a vector given by

$$\mathbf{q} = \frac{(P_i - P_j)}{[(P_i - P_j)_k^2 + \beta]^{1/2}} \quad (4.17)$$

and \mathbf{Q} is a diagonal matrix, with its non-zero values given by

$$\mathbf{Q} = \frac{\beta}{[(P_i - P_j)_k^2 + \beta]^{3/2}} \quad (4.18)$$

By minimizing the functional ϕ_α (Eq. 4.8) with the Total Variation regularization, solutions with abrupt variations between the parameters are preserved.

4.1.3 Matrix \mathbf{S}

For the specific case when there is a configuration with the parameters arranged in the form shown in Figure 4.1, the number of layers is $N=3$, the number of sounding

²The norm l_n of a vector \mathbf{u} is, by definition: $\|\mathbf{u}\|_n = [\sum_{i=1}^N |u_i|^n]^{1/n}$

stations is $N_x=2$, thus the total number of parameters to be estimated by the inversion is $N_p=N \times N_x=6$. The number of differences (or constraints) in the vertical and horizontal directions are $Nd_v = N_p - N_x$ and $Nd_h = N_p - N$, respectively.

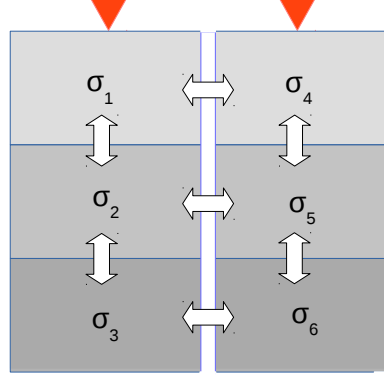


Figure 4.1: Vertical and lateral constraints in a 3-layer model with two adjacent soundings. The red triangles are measuring stations.

$S_{m \times n}$ is a matrix which stores the constraints between the parameters, each line being filled with 1 and -1 in the positions of the pairs of parameters to be related and zeros elsewhere. It is divided into two parts: the upper part contains the vertical constraints and the lower part, the lateral constraints. Therefore, its size is given by a total number of rows equal to $m = Nd_v + Nd_h$ and columns $n = N_p$. For instance, the model shown in Figure 4.1 would produce a S matrix such that:

$$S = \begin{bmatrix} 1 & -1 & 0 & 0 & 0 & 0 \\ 0 & 1 & -1 & 0 & 0 & 0 \\ 0 & 0 & 0 & 1 & -1 & 0 \\ 0 & 0 & 0 & 0 & 1 & -1 \\ 1 & 0 & 0 & -1 & 0 & 0 \\ 0 & 1 & 0 & 0 & -1 & 0 \\ 0 & 0 & 1 & 0 & 0 & -1 \end{bmatrix} \quad (4.19)$$

The result of the multiplication of S matrix with parameters vector \mathbf{P} is equal to another vector with m rows, which stores the differences between the parameters:

$$\begin{bmatrix} 1 & -1 & 0 & 0 & 0 & 0 \\ 0 & 1 & -1 & 0 & 0 & 0 \\ 0 & 0 & 0 & 1 & -1 & 0 \\ 0 & 0 & 0 & 0 & 1 & -1 \\ 1 & 0 & 0 & -1 & 0 & 0 \\ 0 & 1 & 0 & 0 & -1 & 0 \\ 0 & 0 & 1 & 0 & 0 & -1 \end{bmatrix} \begin{bmatrix} P_1 \\ P_2 \\ P_3 \\ P_4 \\ P_5 \\ P_6 \end{bmatrix} = \begin{bmatrix} P_1 - P_2 \\ P_2 - P_3 \\ P_4 - P_5 \\ P_5 - P_6 \\ P_1 - P_4 \\ P_2 - P_5 \\ P_3 - P_6 \end{bmatrix} \quad (4.20)$$

4.2 GAUSS-NEWTON METHOD WITH MARQUARDT'S STRATEGY

The objective function ϕ_α (Eq. 4.8) is treated as a second order approximation $\hat{\phi}_\alpha$ of ϕ_α around point \mathbf{P}_k , with the second order and higher derivatives equal to zero, since the non-linear geophysical functional is approximated by a linear function in \mathbf{P} .

$$\hat{\phi}_\alpha(\mathbf{P}) \simeq \phi_\alpha(\mathbf{P}_k) + \Delta\mathbf{P}_k^t \mathbf{g}_k^\alpha + \frac{1}{2} \Delta\mathbf{P}_k^t \mathbf{H}_k^\alpha \Delta\mathbf{P} \quad (4.21)$$

where $\Delta\mathbf{P}_k$ is the perturbation vector of the parameters, in the k -th iteration, and

$$\mathbf{g}_k^\alpha = (\nabla_{\mathbf{P}} \phi_\alpha) |_{\mathbf{P}=\mathbf{P}_k}, \quad (4.22)$$

$$\mathbf{H}_k^\alpha = (\nabla \nabla_{\mathbf{P}}^t \phi_\alpha) |_{\mathbf{P}=\mathbf{P}_k} \quad (4.23)$$

are, respectively, the gradient vector and the Hessian (second derivative matrix) of the functional ϕ_α , both with respect to the vector \mathbf{P} evaluated in \mathbf{P}_k .

From the expansion of the functional ϕ_α in a Taylor series (Eq. 4.21) and taking into account that $\mathbf{g}_k^\alpha = \mathbf{g}_k^d + \alpha \mathbf{g}_k^{REG}$ and $\mathbf{H}_k^\alpha = \mathbf{H}_k^d + \alpha \mathbf{H}_k^{REG}$, we can rewrite Eq. 4.21 as:

$$\hat{\phi}_\alpha(\mathbf{P}) \simeq \phi_\alpha(\mathbf{P}_k) + \Delta\mathbf{P}_k^t (\mathbf{g}_k^d + \alpha \mathbf{g}_k^{REG}) + \frac{1}{2} \Delta\mathbf{P}_k^t (\mathbf{H}_k^d + \alpha \mathbf{H}_k^{REG}) \Delta\mathbf{P}. \quad (4.24)$$

where the gradient and Hessian of the data misfit functional are approximated by (Pujol, 2007):

$$\mathbf{g}_k^d = -2\mathbf{A}^t [\mathbf{d} - \mathbf{F}(\mathbf{P})] \quad (4.25)$$

$$\mathbf{H}_k^d = 2\mathbf{A}^t \mathbf{A} \quad (4.26)$$

For the EMMF and CSAMT joint inversion, for example, $\mathbf{g}_k^d = [\mathbf{g}_k^{\text{EMMF}}, \mathbf{g}_k^{\text{CSAMT}}]$ and $\mathbf{H}_k^d = [\mathbf{H}_k^{\text{EMMF}}, \mathbf{H}_k^{\text{CSAMT}}]$. The \mathbf{g}^{REG} and \mathbf{H}^{REG} are the gradient vector and the Hessian of the regularization functional, which can be either eqs. 4.10 or 4.15 for the gradient term and 4.11 or 4.16 for the Hessian.

To obtain the necessary step $\Delta\mathbf{P}_k$ to find the minimum of the functional $\hat{\phi}_\alpha(\mathbf{P})$, its gradient vector (with respect to vector $\Delta\mathbf{P}_k$) is calculated and equated to the null vector, which results in:

$$(2\mathbf{A}^t \mathbf{A} + \alpha \mathbf{H}^{REG}) \Delta\mathbf{P} = 2\mathbf{A}^t [\mathbf{d} - \mathbf{F}(\mathbf{P})] - \alpha \mathbf{g}^{REG}, \quad (4.27)$$

where \mathbf{A} is the Jacobian or sensitivity matrix, defined as:

$$\mathbf{A}_{ij} = \frac{\partial \mathbf{F}_i(\mathbf{p})}{\partial p_j} = \frac{\partial \mathbf{F}_i(\mathbf{p})}{\partial \ln(\sigma_j)} = \sigma_j \frac{\partial \mathbf{F}_i(\mathbf{p})}{\partial \sigma_j} \quad (4.28)$$

\mathbf{A}_{ij} denotes the sensitivity of the i -th data with respect to the j -th parameter. In this

work, the Jacobian matrix was built by calculating the analytical derivatives of the 1D EM responses with respect to conductivities (eq. 4.28). With that, the performance of the code is improved one order of magnitude faster than conventional numerical methods (Crepaldi et al., 2011).

Thus, in the k -th iteration, Eq. 4.27 is solved for $\Delta\mathbf{P}_k$ and the updated value of the parameter vector will be

$$\mathbf{P}_{k+1} = \mathbf{P}_k + \Delta\mathbf{P}_k \quad (4.29)$$

Marquardt (1963) suggests adding a factor λ (Marquardt coefficient) to the diagonal of the Hessian matrix to stabilize the steps of the process. It is a positive scalar and its value is changed during the inversion process, according to the analysis of the objective function $\hat{\phi}_\alpha$, in a given estimate, in relation to the previous estimate. If the objective function decreases ($\phi_\alpha(\mathbf{P}_{k+1}) < \phi_\alpha(\mathbf{P}_k)$), λ changes to $\frac{\lambda}{10}$. If the objective function increases ($\phi_\alpha(\mathbf{P}_{k+1}) > \phi_\alpha(\mathbf{P}_k)$), λ changes to 10λ . After the addition of the Marquardt parameter, Eq. 4.27 turns to:

$$(2\mathbf{A}^t\mathbf{A} + \alpha\mathbf{H}^{REG} + \lambda\mathbf{I})\Delta\mathbf{P} = 2\mathbf{A}^t(\mathbf{d} - \mathbf{F}(\mathbf{P})) - \alpha\mathbf{g}^{REG} \quad (4.30)$$

where \mathbf{I} is the identity matrix and the updated value of the parameter vector will be given by Eq. 4.29.

At a given iteration, if the objective function is close to the minimum, λ is sufficiently small compared to the elements of the Hessian and the method is closest to the Gauss-Newton method (Eq. 4.27). On the other hand, in regions far from the minimum point, λ becomes large compared to the elements of the Hessian, making the matrix $(2\mathbf{A}^t\mathbf{A} + \alpha\mathbf{H}^{REG} + \lambda\mathbf{I})$ diagonally dominant, and the iteration simply takes a small step in the downward direction of the gradient of $\hat{\phi}_\alpha$ (as in the Steepest Descent method).

4.3 ANALYTICAL DERIVATIVES

The interpretative model used to calculate sensitivities is a plane-parallel layered medium (Fig. 3.1), with a total of 25 layers including the infinite substrate. The thicknesses of each layer increases 10% with depth, starting with a 10 m thick first layer. It consists of an homogeneous half-space, hence all layers have the same conductivities equal to $200 \Omega.m$.

The following notation is used for the parameters of layer j : Z_j and χ_j are the intrinsic impedance and admittance, respectively; \hat{Z}_j and $\hat{\chi}_j$ are the apparent impedance and admittance at the interface on top of the layer; h_j is the thickness of the layer; $u_j = \sqrt{k_r^2 - k_j^2}$ and $k_j^2 = -\eta_j\zeta_j$, where $\eta_j = \sigma_j + i\omega\epsilon_j$ and $\zeta_j = i\omega\mu_j$. For this specific case, the electric permittivity ϵ_j and magnetic permeability μ_j of each layer are considered to be constant and equal to their respective values in free-space ($\epsilon_0 = 8.854 \times 10^{-12}$; $\mu_0 = 4\pi \times 10^{-7}$)

Figure 4.2 show the sensitivities for each observation corresponding to their respective method.

4.3.1 EMMF

To calculate the sensitivity matrix (Eq. 4.28) for the EMMF case, we need the derivative of the radial magnetic field with respect to the conductivities of the interpretative model:

$$\mathbf{A}_{ij} = \sigma_j \frac{\partial(\bar{H}_r^{(0)})_i}{\partial\sigma_j} \quad (4.31)$$

$$\frac{\partial\bar{H}_r^{(0)}}{\partial\sigma_j} = \frac{1}{H_z^0} \int_0^\infty \chi_0 E_0 \frac{\partial R_{TE}^{(0)}}{\partial\sigma_j} J_1(k_r r) k_r dk_r \quad (4.32)$$

where the derivative of the reflection coefficient at the surface with respect to the model conductivities is:

$$\frac{\partial R_{TE}^{(0)}}{\partial\sigma_j} = \frac{-2\chi_0}{(\chi_0 + \hat{\chi}_1)^2} \frac{\partial\hat{\chi}_1}{\partial\sigma_j} \quad (4.33)$$

and the derivative of the surface apparent admittance with respect to the model conductivities $\frac{\partial\hat{\chi}_1}{\partial\sigma_j}$ is calculated using the following recursive formula:

For $m \neq j$

$$\frac{\partial\hat{\chi}_m}{\partial\sigma_j} = \frac{\chi_m^2 \operatorname{sech}^2(u_m h_m)}{(\chi_m + \hat{\chi}_{m+1} \tanh(u_m h_m))^2} \frac{\partial\hat{\chi}_{m+1}}{\partial\sigma_j}; \quad (4.34)$$

For $m = j \neq N$

$$\begin{aligned} \frac{\partial\hat{\chi}_m}{\partial\sigma_j} &= \frac{\frac{\partial\hat{\chi}_{j+1}}{\partial\sigma_j} + \frac{\chi_j h_j \operatorname{sech}^2(u_j h_j)}{2} + \frac{\tanh(u_j h_j)}{\zeta_j}}{\chi_j + \hat{\chi}_{j+1} \tanh(u_j h_j)} \\ &= \frac{(\frac{1}{2u_j} + \frac{h_j \hat{\chi}_{j+1} \operatorname{sech}^2(u_j h_j)}{2\chi_j})(\hat{\chi}_{j+1} \chi_j + \chi_j^2 \tanh(u_j h_j))}{(\chi_j + \hat{\chi}_{j+1} \tanh(u_j h_j))^2}; \end{aligned} \quad (4.35)$$

For $m = j = N$

$$\frac{\partial\hat{\chi}_N}{\partial\sigma_N} = \frac{\partial\chi_N}{\partial\sigma_N}; \quad (4.36)$$

with

$$\frac{\partial\chi_m}{\partial\sigma_j} = \frac{1}{2u_j}. \quad (4.37)$$

4.3.2 CSAMT

The sensitivity matrix for the CSAMT case depends on the derivative of the radial electric field with respect to the conductivities of the interpretative model:

$$\mathbf{A}_{ij} = \sigma_j \frac{\partial(\bar{E}_x^{(0)})_i}{\partial\sigma_j} \quad (4.38)$$

$$\begin{aligned} \frac{\partial E_x^{(0)}}{\partial\sigma_j} = & -\frac{IdS_x}{4\pi} \left(\frac{1}{r} - \frac{2x^2}{r^3} \right) \int_0^\infty \left[-\frac{\partial R_{TM}^{(0)}}{\partial\sigma_j} \right] Z_0 J_1(k_r r) dk_r \\ & -\frac{IdS_x}{4\pi} \frac{x^2}{r^2} \int_0^\infty \left[-\frac{\partial R_{TM}^{(0)}}{\partial\sigma_j} \right] Z_0 J_0(k_r r) k_r dk_r \\ & -\frac{IdS_x}{4\pi} \left(\frac{1}{r} - \frac{2y^2}{r^3} \right) \int_0^\infty \frac{\partial R_{TE}^{(0)}}{\partial\sigma_j} \frac{1}{\chi_0} J_1(k_r r) dk_r \\ & -\frac{IdS_x}{4\pi} \frac{y^2}{r^2} \int_0^\infty \frac{\partial R_{TE}^{(0)}}{\partial\sigma_j} \frac{1}{\chi_0} J_0(k_r r) k_r dk_r \end{aligned} \quad (4.39)$$

where $\frac{\partial R_{TE}^{(0)}}{\partial\sigma_j}$ is given by 4.33 and $\frac{\partial R_{TM}^{(0)}}{\partial\sigma_j}$ is given by:

$$\frac{\partial R_{TM}^{(0)}}{\partial\sigma_j} = \frac{-2Z_0}{(Z_0 + \hat{Z}_1)^2} \frac{\partial \hat{Z}_1}{\partial\sigma_j} \quad (4.40)$$

and the derivative of the surface apparent impedance with respect to the model parameters $\frac{\partial \hat{Z}_1}{\partial\sigma_j}$ is calculated using the recursive formula:

For $m \neq j$

$$\frac{\partial \hat{Z}_m}{\partial\sigma_j} = \frac{Z_m^2 \operatorname{sech}^2(u_m h_m)}{(Z_m + \hat{Z}_{m+1} \tanh(u_m h_m))^2} \frac{\partial \hat{Z}_{m+1}}{\partial\sigma_j}; \quad (4.41)$$

For $m = j \neq N$

$$\begin{aligned} \frac{\partial \hat{Z}_m}{\partial\sigma_j} = & \frac{\frac{\partial Z_m}{\partial\sigma_j} \hat{Z}_{j+1} + 2Z_j \frac{\partial Z_m}{\partial\sigma_j} \tanh(u_j h_j) + Z_j^2 \operatorname{sech}^2(u_j h_j) h_j \zeta_j}{2u_j (Z_j + \hat{Z}_{j+1} \tanh(u_j h_j))} \\ & \frac{(\frac{\partial Z_m}{\partial\sigma_j} + \hat{Z}_{j+1} \operatorname{sech}^2(u_j h_j) h_j \zeta_j) (\hat{Z}_{j+1} Z_j + Z_j^2 \tanh(u_j h_j))}{2u_j (Z_j + \hat{Z}_{j+1} \tanh(u_j h_j))^2}; \end{aligned} \quad (4.42)$$

For $m = j = N$

$$\frac{\partial \hat{Z}_N}{\partial\sigma_N} = \frac{\partial Z_N}{\partial\sigma_N}; \quad (4.43)$$

with

$$\frac{\partial Z_m}{\partial\sigma_j} = \frac{\zeta_j}{2u_j \sigma_j} - \frac{u_j}{\sigma_j^2}. \quad (4.44)$$

4.3.3 MT

For the MT case, the sensitivity matrix is:

$$\mathbf{A}_{ij} = \sigma_j \frac{\partial(\hat{Z}_1)_i}{\partial\sigma_j} \quad (4.45)$$

where the term $\frac{\partial\hat{Z}_1}{\partial\sigma_j}$ is calculated using the set of equations 4.41, 4.42, 4.43 and 4.44.

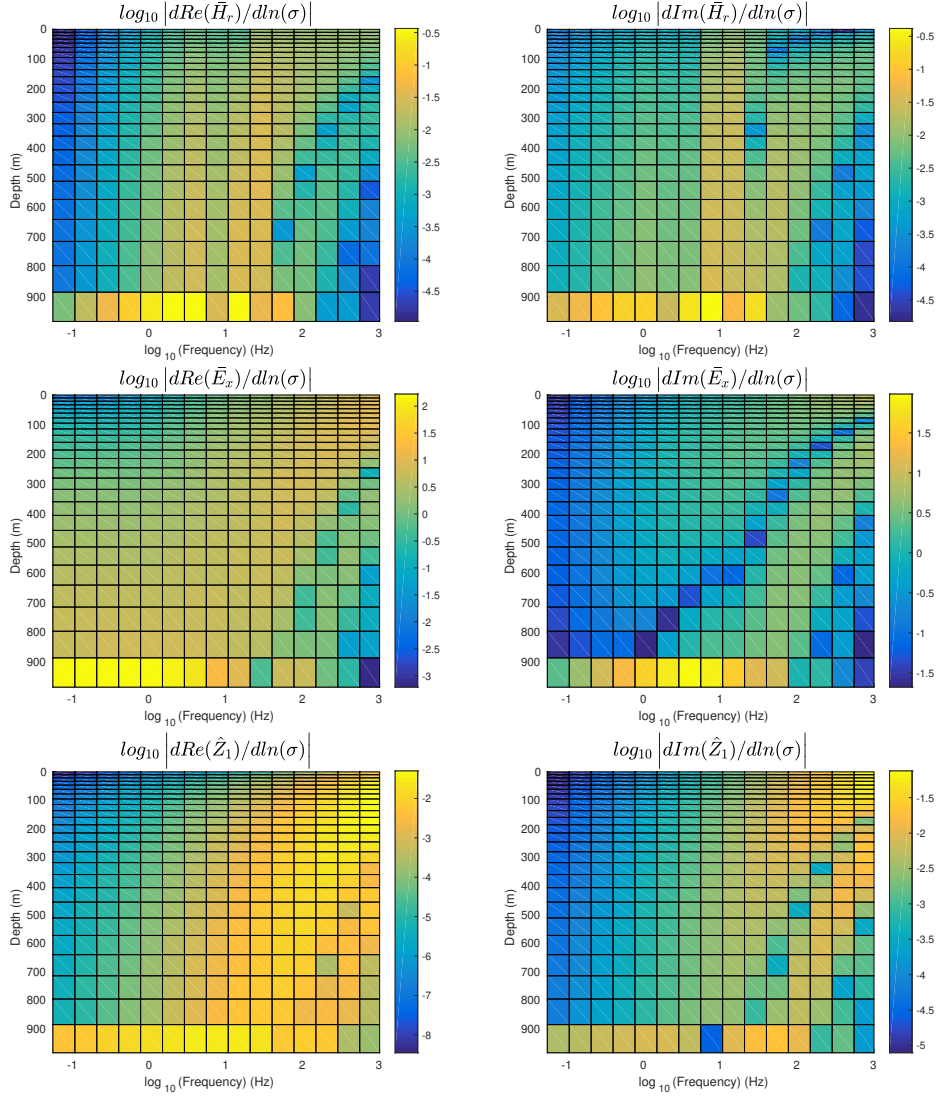


Figure 4.2: Sensitivities calculated for the EMMF, CSAMT and MT observations. Each column corresponds to the sensitivity of a layered medium at a specific frequency. The vertical axis is the depth of the interpretative model interfaces.

5 1D INVERSION RESULTS

The synthetic data for the 1D inversion were generated by the model presented in figure 5.1. Two cases were analyzed: Model 1 consists of a conductive target layer ($10 \Omega\cdot\text{m}$) and Model 2, of a resistive ($500 \Omega\cdot\text{m}$) layer, both 200 m thick and embedded in a background medium with $100 \Omega\cdot\text{m}$ resistivity. Responses were recorded at a fixed position of $x = 7 \text{ km}$, by 15 logarithmically spaced frequencies in the range of 0.1 Hz to 1000 Hz. A circular loop with radius of 340 m was used to simulate the EMMF source.

The interpretative model used is a layered medium similar to the one presented in Figure 3.1, with a total of 25 layers including the infinite substrate. The thicknesses of each layer increases 10% with depth, starting with a 10 m thick first layer. Their conductivities start as an initial guess represented by the dashed red lines and their estimated values (after the inversion) are shown by the black lines in “stairs” format. The stability of the final models was tested by analyzing if they would be obtained if the process was started using different resistivity values for the layers of the initial interpretative model.

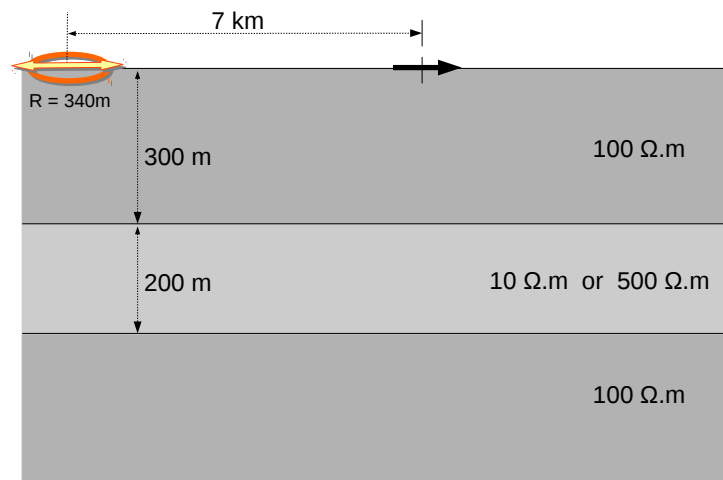


Figure 5.1: 1D Model used to generate the 1D synthetic data. The field measurements were taken at $x = 7 \text{ km}$.

5.1 MODEL 1

Figures 5.2 and 5.3 show the 1D models obtained using the GS and TV regularizations, respectively. In these figures, the three results in the first row correspond to separate inversions of EMMF, CSAMT and MT methods while the second row contains the 1D joint inversion results. Overall, the models estimated by joint inversions using TV were significantly better than the smooth ones obtained with GS for Model 1. Not only the conductive layer was identified, but also its boundaries were delineated and the resistivity of the background was correctly defined.

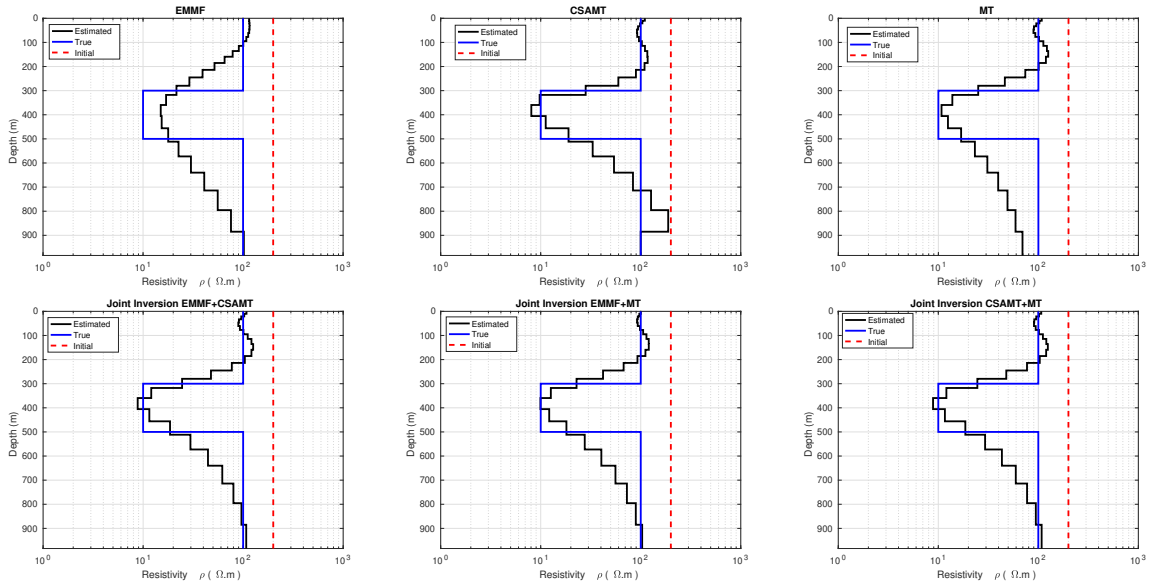


Figure 5.2: Final 1D models obtained by isolated and joint inversion of the EMMF, CSAMT and MT methods using the Global Smoothness regularization. The conductivities of each layer start as an initial guess represented by the dashed red lines and their estimated values (after the inversion) are shown by the black lines in “stairs” format.

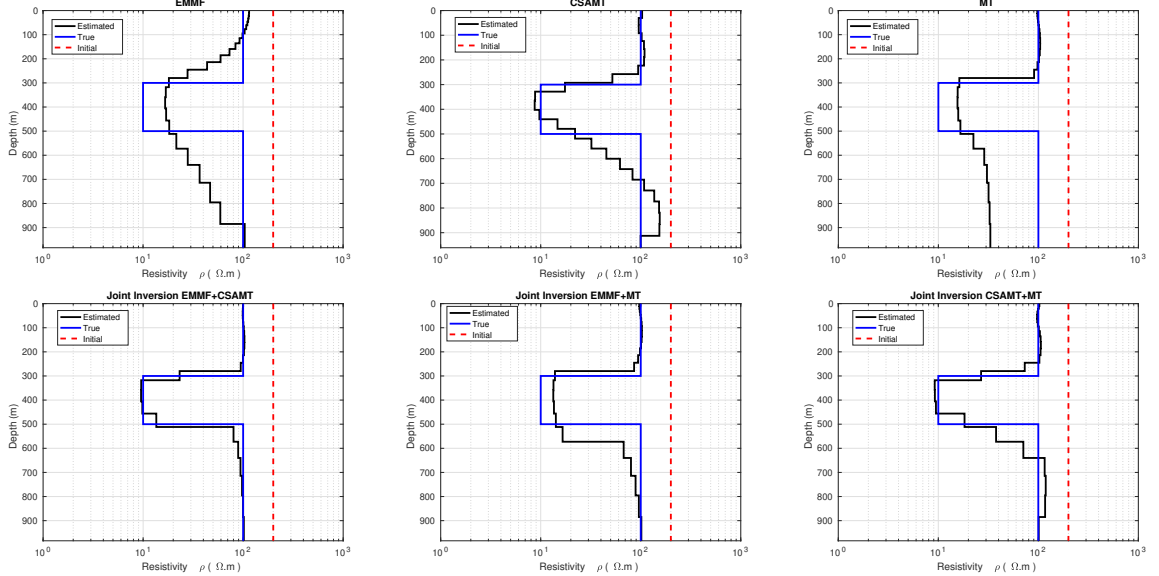


Figure 5.3: Final 1D models obtained by isolated and joint inversion of the EMMF, CSAMT and MT methods using the Total Variation regularization.

Specifically analyzing each result for **Model 1**:

- EMMF - Despite those results illustrate a good attempt to resolve the resistivities of the target layer and background, this is done in a over smoothed way thus the conductive layer interfaces were not well-resolved even in the TV case.
- CSAMT - The isolated CSAMT inversions are good in terms of reaching the correct

resistivity of the target layer. The background resistivity, however, was significantly affected by an expected oscillatory effect caused by the regularizations.

- MT - Both the upper background and the target conductive layer were correctly resolved, whereas the resistivities obtained for the lower background area were not sufficiently high as a result of the influence of the vertical regularization which spreads down through the deeper layers of the interpretative model.
- EMMF+CSAMT - The 1D joint inversion using GS improves the over smoothness problem present in the EMMF isolated inversion and the background resistivity is corrected for the oscillatory effect mentioned in the CSAMT isolated inversion. Nevertheless, the model obtained by 1D joint inversion using TV is significantly closer to the true model, since this regularization is efficient to delineate the interfaces of the conductive layer. This was the best result because it matched almost perfectly the true model.
- EMMF+MT - Same analysis is done for this joint inversion: the over smoothness problem and the lower background area are corrected reaching sufficiently high resistivities in this case. The TV result is better than the GS one since it provided a model similar to the true model, despite the fact that it was slightly thicker.
- CSAMT+MT - The CSAMT contributed in this result by correcting the area under the conductive layer, which wasn't well resolved in the MT-only inversion. The oscillatory effect in the CSAMT-only is also attenuated in this case.

5.2 MODEL 2

Model 2 is shown in Figure 5.1, corresponding to the case when the heterogeneity is resistive. The estimated models obtained with the GS and TV regularizations are in Figures 5.4 and 5.5, respectively. Model 2, unlike Model 1 which had better estimated models by joint inversions using TV, had sufficiently good estimated models by the inversion of the CSAMT data alone. It was sufficient to recover the target location both using the GS and TV since in this case we are dealing with the TM mode components which exhibit a special interaction with resistive horizontal interfaces, resulting in surface charge density (Crepaldi et al., 2011).

The EMMF and MT methods showed a minimal sensitivity to the resistive layer, being efficient and contributing only in the determination of the host medium. In the EMMF case, it can be explained by the fact that the EMMF data are composed of the radial magnetic component of the coil, which is strongly influenced by the inductive effects of the geological environment. Therefore it responds more efficiently to conductive targets, since those structures suffer a greater induction effect.

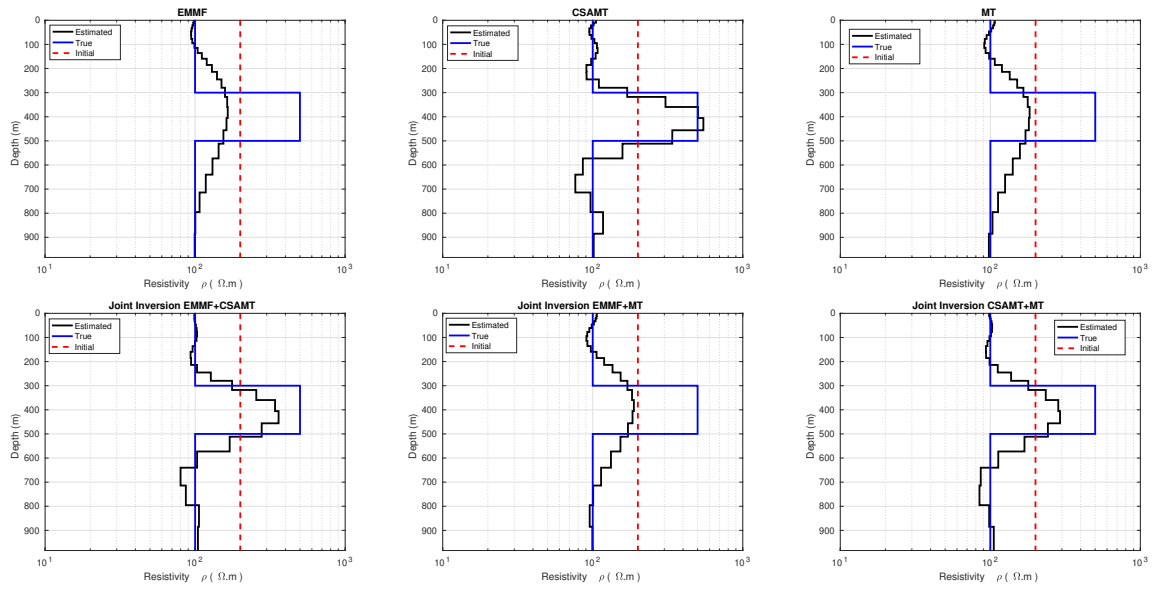


Figure 5.4: Final 1D models obtained by isolated and joint inversion of the EMMF, CSAMT and MT methods using the Global Smoothness regularization.

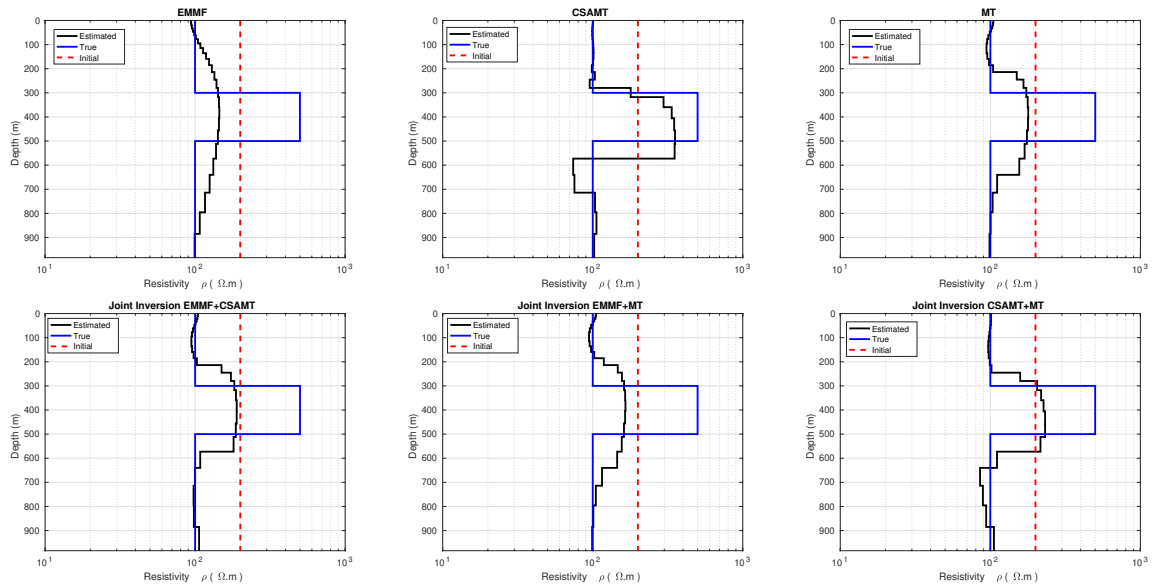


Figure 5.5: Final 1D models obtained by isolated and joint inversion of the EMMF, CSAMT and MT methods using the Total Variation regularization.

Specifically analyzing each result for **Model 2**:

- EMMF - The EMMF method alone did not provided good results in terms of the identification of the resistive layer. Although it could resolve the background relatively well, it was almost insensitive to the target layer.
- CSAMT - Despite some oscillations on the background resistivities, the isolated CSAMT inversions were enough to determine an estimated model sufficiently close to the true one.
- MT - Similar to the EMMF method, MT could resolve the background resistivity well, but the results were not good in terms of the identification of the resistive layer.
- EMMF+CSAMT - The 1D joint inversion results showed a better attempt to get the resistivities of the target layer if compared to the EMMF isolated inversion results, this was done by the contribution of the CSAMT data. The background resistivity was improved in the TV result.
- EMMF+MT - There were no significant improvements if compared to the corresponding separate inversions. The results were similar to the ones obtained by the isolated inversion of these two methods.
- CSAMT+MT - The layer interfaces were identified and the background oscillations in the CSAMT were attenuated due to the contribution of MT.

6 LCI RESULTS

To illustrate the use of the inversion algorithm, we present its application to three different sets of synthetic data generated by 2D forward modeling finite element programs written by Silva (2012) - EMMF and Perez (2016) - CSAMT. All datasets comprise 26 equally spaced measuring stations, going from 4500 m to 9500 m, with 15 logarithmically spaced frequencies in the range of 0.1 Hz to 1000 Hz. The synthetic data of each problem were contaminated with 2% Gaussian noise. Moreover, the stability of the solution was tested by performing the inversion starting with different initial values for the resistivity of the interpretative models and analyzing whether a similar final model were obtained from these.

6.1 MODEL 1

The inversion algorithms were tested in a first model consisting of a resistive semi-space with a conductive target body ($10 \Omega.m$) embedded in it, as observed in figure 6.1. The resistivity of the half-space is $\rho_1 = 100 \Omega.m$ while the heterogeneity has $\rho_2 = 10 \Omega.m$.

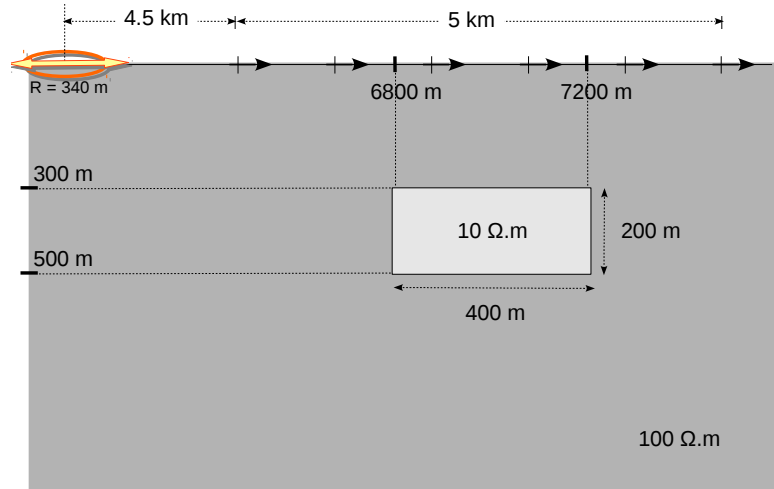


Figure 6.1: 2D Model. The field measurements were taken along a 5 km survey line at the surface, starting at $x = 4500$ m with a receiver spacing of 200 m.

Figure 6.2 shows the observed data obtained from this 2D model. As mentioned in the Methodology (chapter 2), the observations are:

1. EMMF: the real and imaginary components of the radial horizontal magnetic field normalized by the vertical component of a magnetic dipole (\bar{H}_r);
2. CSAMT: the real and imaginary components of the radial electrical field normalized by its dipole moment and a factor to correct the geometric attenuation with distance (\bar{E}_x);

3. MT: the real and imaginary components of the apparent impedance tensor at the surface (\hat{Z}_1).

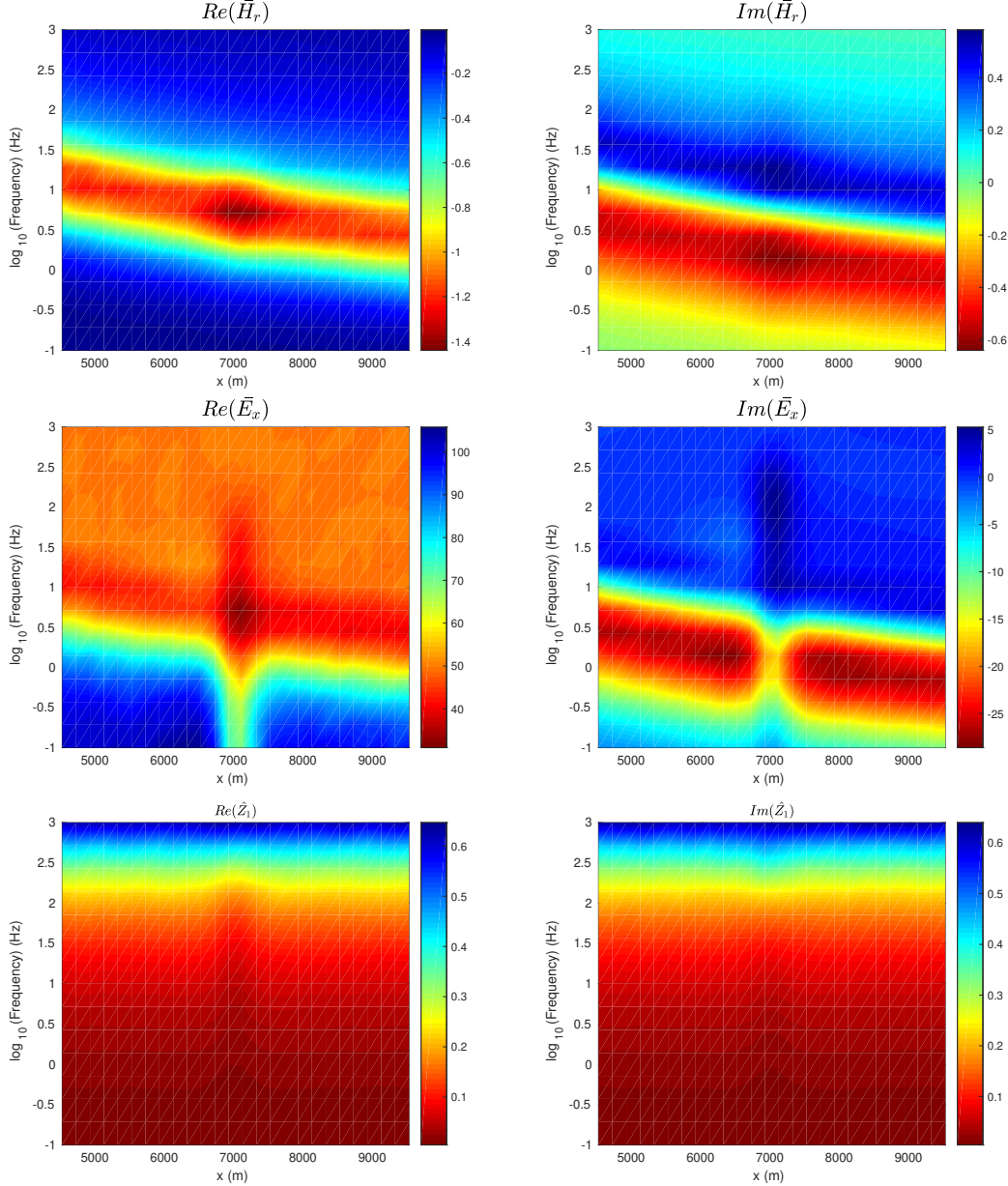


Figure 6.2: EMMF, CSAMT and MT synthetic observed data generated from Model 1.

Figures 6.3 and 6.4 show the pseudo-2D models obtained using the LCI technique and the GS and TV regularizations, respectively. Overall, similar to the results from 1D inversion shown in section 5.1 of chapter 5, the models estimated by joint LCI using both GS and TV were good enough in the sense of detecting the presence of the 2D conductive body. The individual inversions of CSAMT and EMMF present particular problems that will be discussed in the following paragraphs. The isolated MT LCI, on the other hand, was as good as the joint inversions since the nature of magnetotelluric fields are plane-waves and data from this method is intrinsically easier to be fitted by 1D models which

may have benefited its results produced by LCI methodology.

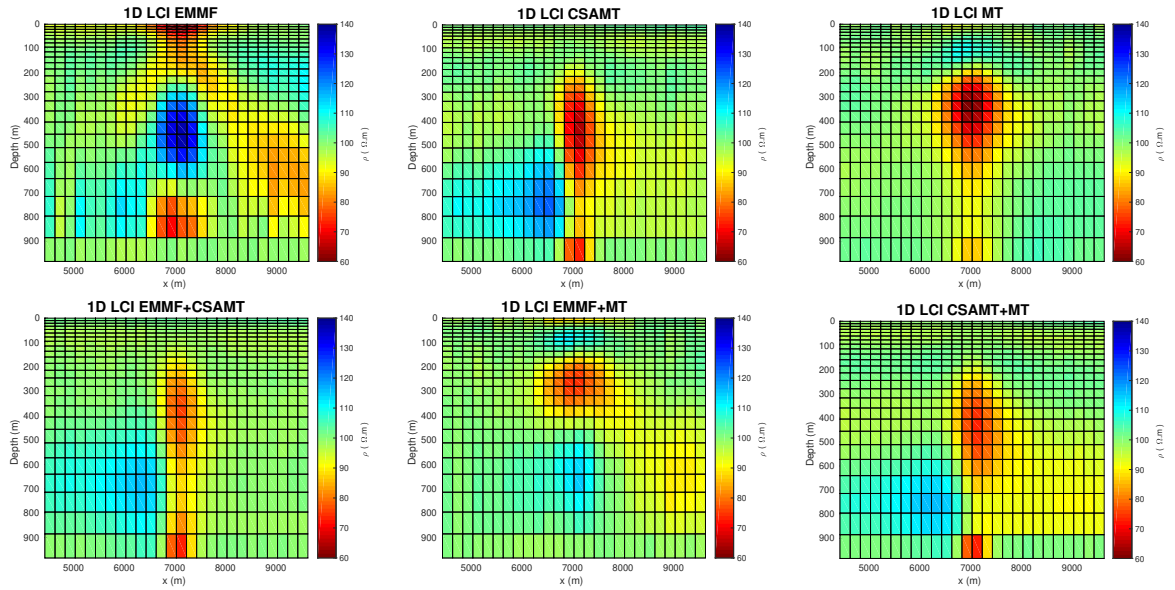


Figure 6.3: Final pseudo-2D models obtained by isolated and joint inversion of the EMMF, CSAMT and MT methods using the Global Smoothness regularization.

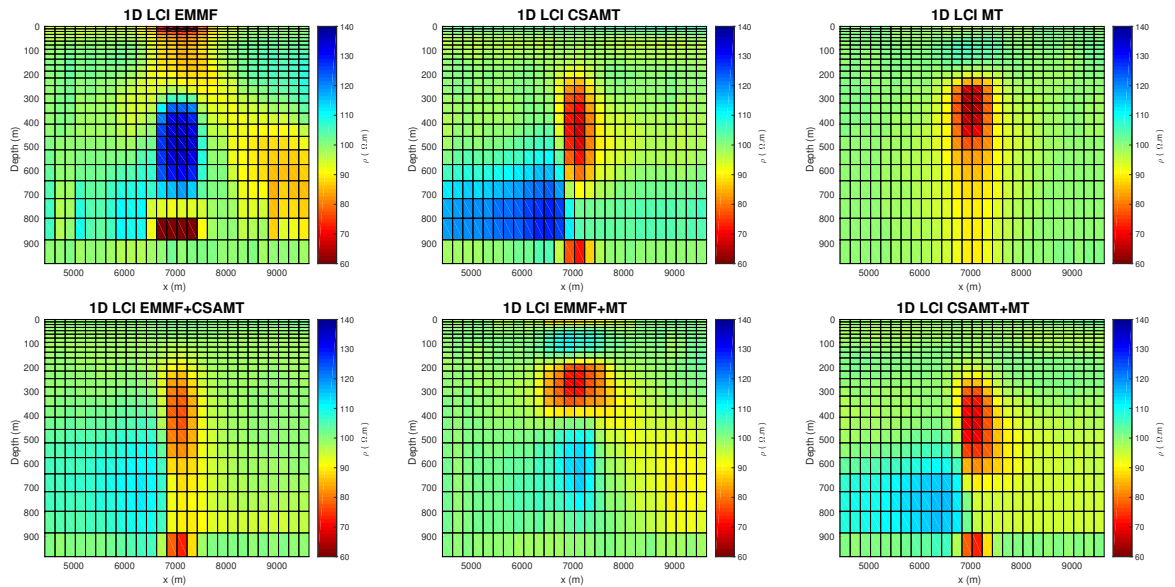


Figure 6.4: Final pseudo-2D models obtained by isolated and joint inversion of the EMMF, CSAMT and MT methods using the Total Variation regularization.

Specifically analyzing each result for **Model 1**:

- EMMF - Instead of a conductive body, the individual EMMF LCI generated a model with a resistive body and some conductive artifacts in the background. After careful analysis, it was considered to be a case when the 2D nature of the fields imposed itself on the observations and that was the best model that could fit the observed data taking into account the fact that the calculated data was generated by a set of 1D layered interpretative models. The low conductivity areas right above and under the heterogeneity are artifacts created by the 1D inversion (features similar to these are observed in Kang et al. (2013)).
- CSAMT - The individual CSAMT LCI identified the heterogeneity correctly as a conductive body, despite a more resistive effect on the left hand side area under the body. This resistivity anomaly is probably due to the shadow effect, a common feature in CSAMT data (Zonge and Hughes, 1991).
- MT - The effect of the vertical constraint, that spread the influence of the conductive bodies down through the deeper layers, is now balanced by the influence of the lateral constraints, so the 2D body is better delineated using the LCI.
- EMMF+CSAMT - This joint LCI result improved the final model by attenuating the artifacts mentioned in the isolated LCI of these two methods.
- EMMF+MT - This inversion also attenuated artifacts in the background resistivity, however it located the conductive body shallower and smaller (in the vertical direction) than it is in reality.
- CSAMT+MT - It locates the 2D body correctly, addressing correct resistivities to both the target and the background medium. There is an effect spread laterally (due to the lateral constraints) causing a slightly uncorrect resistivity for the area under the body.

6.2 MODEL 2

Second model tested is geometrically equal to the first one (fig. 6.1), except for the fact that the 2D body is resistive now ($\rho_2 = 500 \Omega.m$). Apart from the resistivity of the target, same configuration was used to simulate the data acquisition.

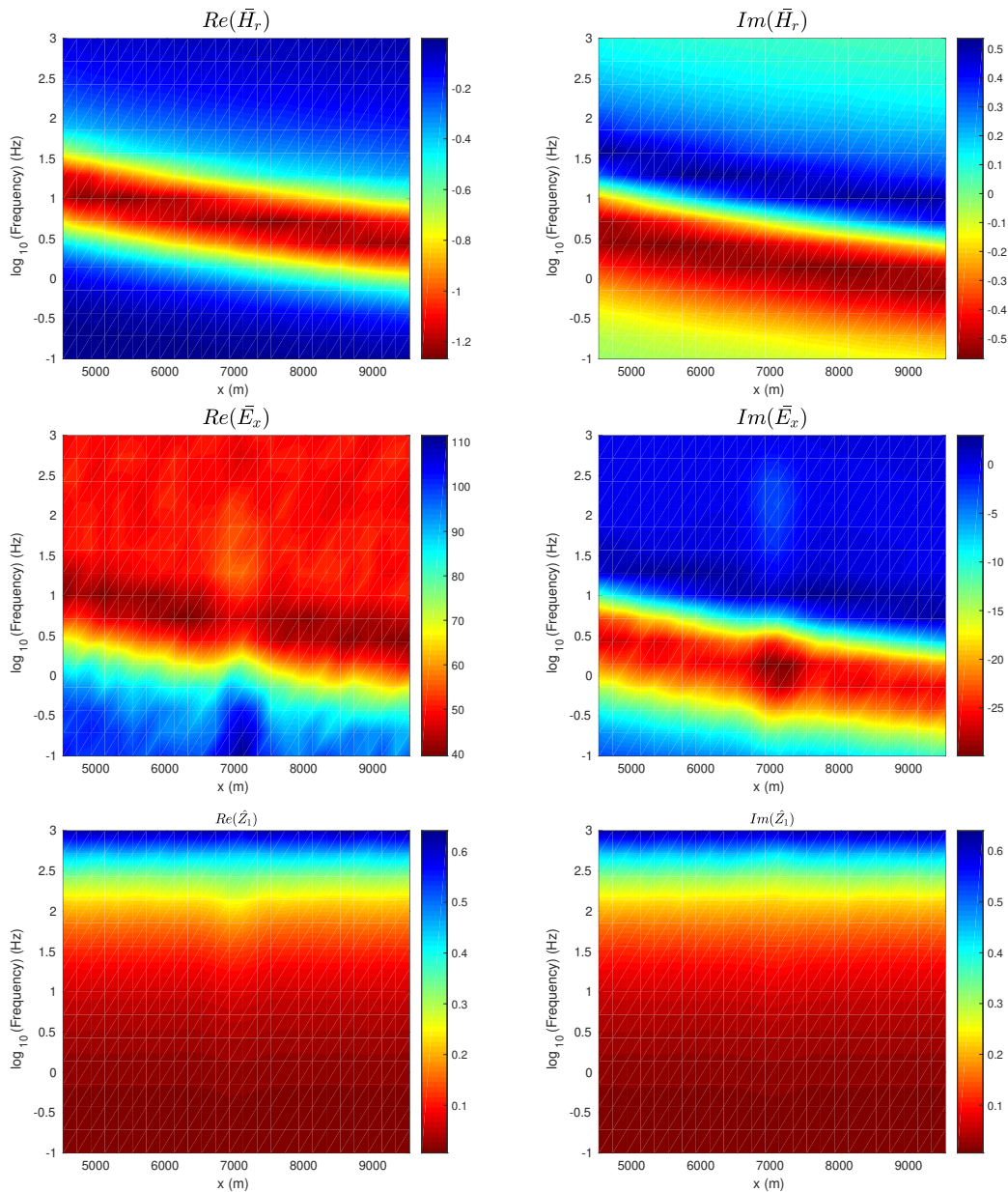


Figure 6.5: EMMF, CSAMT and MT synthetic observed data generated from Model 2.

Figures 6.6 and 6.7 show the pseudo-2D models obtained using the LCI technique and the GS and TV regularizations, respectively. Similar to the results from 1D inversion shown in section 5.2 of chapter 5, the individual CSAMT inversion was sufficient to detect the target resistive body, however there were some unwanted artifacts in the resistivities of the medium that hosts this target. The models estimated by EMMF+CSAMT joint inversion had these artifacts attenuated due to the influence of the EMMF which resolved the background.

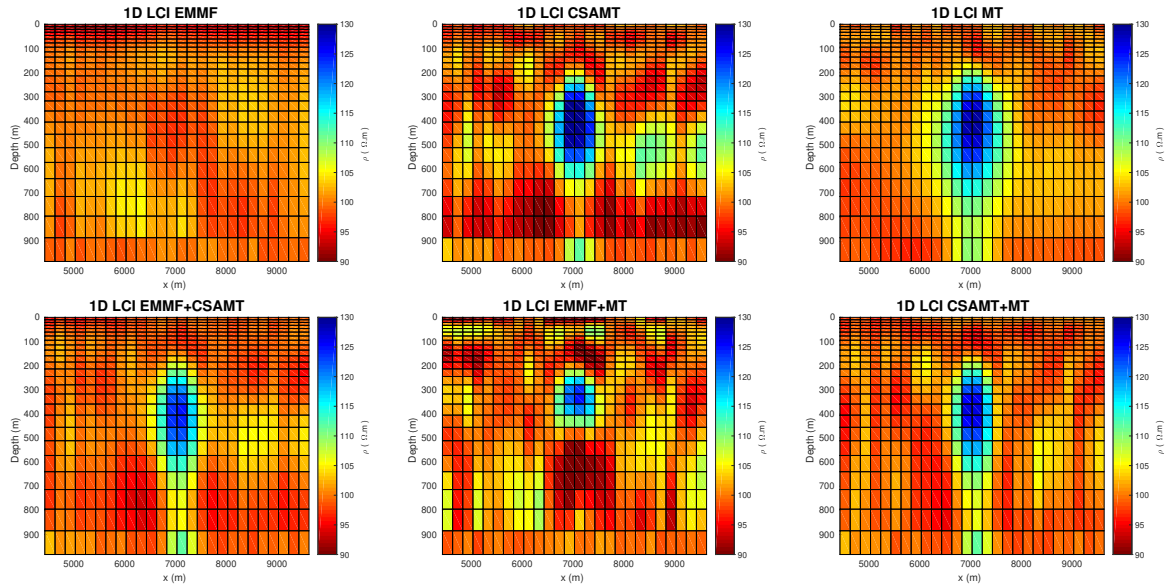


Figure 6.6: Final pseudo-2D models obtained by isolated and joint inversion of the EMMF, CSAMT and MT methods using the Global Smoothness regularization.

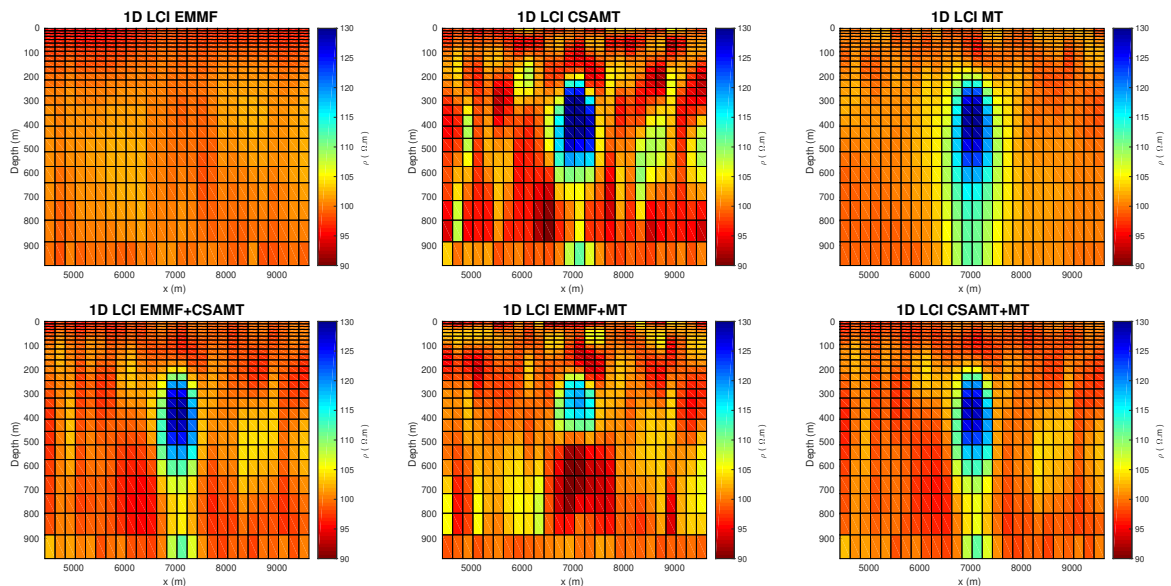


Figure 6.7: Final pseudo-2D models obtained by isolated and joint inversion of the EMMF, CSAMT and MT methods using the Total Variation regularization.

Specifically analyzing each result for **Model 2**:

- EMMF - The EMMF method alone did not provide good results in terms of the identification of the resistive body. It could resolve the background relatively well, however it was unable to identify the target. This can be explained by the fact that EMMF's observations are the radial magnetic components of the coil, which are strongly influenced by the inductive effects, hence it does not have a good response when the medium is resistive because those structures are intrinsically resistant to induction effects.

- CSAMT - The individual CSAMT LCI positioned the heterogeneity correctly and the background resistivities were approximately the correct ones, even though some oscillations impaired this result.
- MT - As mentioned before, the individual MT LCI was as good as the joint inversions since the nature of magnetotelluric fields are plane-waves and data from this method is intrinsically easier to be fitted by 1D models.
- EMMF+CSAMT - This result suggests that the joint LCI of EMMF and CSAMT is an excellent technique in the exploration of resistive structures. These methods provide complementary information, since 1- the EMMF is largely insensitive to resistive bodies, but can resolve the background regional resistivity structure and 2- the CSAMT method responds to resistive targets because of vertical electric currents from its electric dipole source fields, but its isolated inversion showed an unwanted oscillation effect in the resistivities of the background.
- EMMF+MT - Similar to what happened in the first model, with a conductive target, this inversion located the conductive body shallower and smaller than the real model.
- CSAMT+MT - The influence of the MT data helped the regional resistivities from the background. Additionally, the heterogeneity was quite well resolved thus this joint LCI also proved to be a good option in the search for resistive structures.

6.3 MODEL 3

Figures 6.8 and 6.9 show the third model tested in this study and its corresponding data pseudo sections. It is a two-layer model containing one conductive body ($\rho_1 = 10 \Omega.m$) located in the upper layer ($\rho_2 = 100 \Omega.m$). The substrate is an infinite resistive layer of $\rho_3 = 500 \Omega.m$.

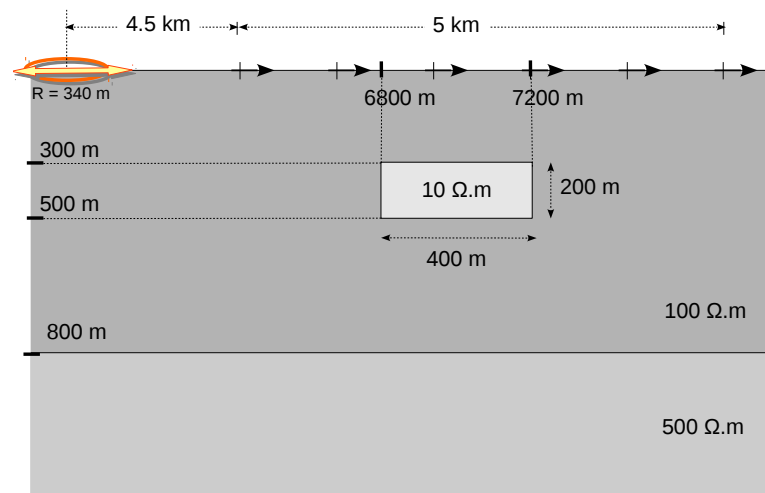


Figure 6.8: 2D Model.

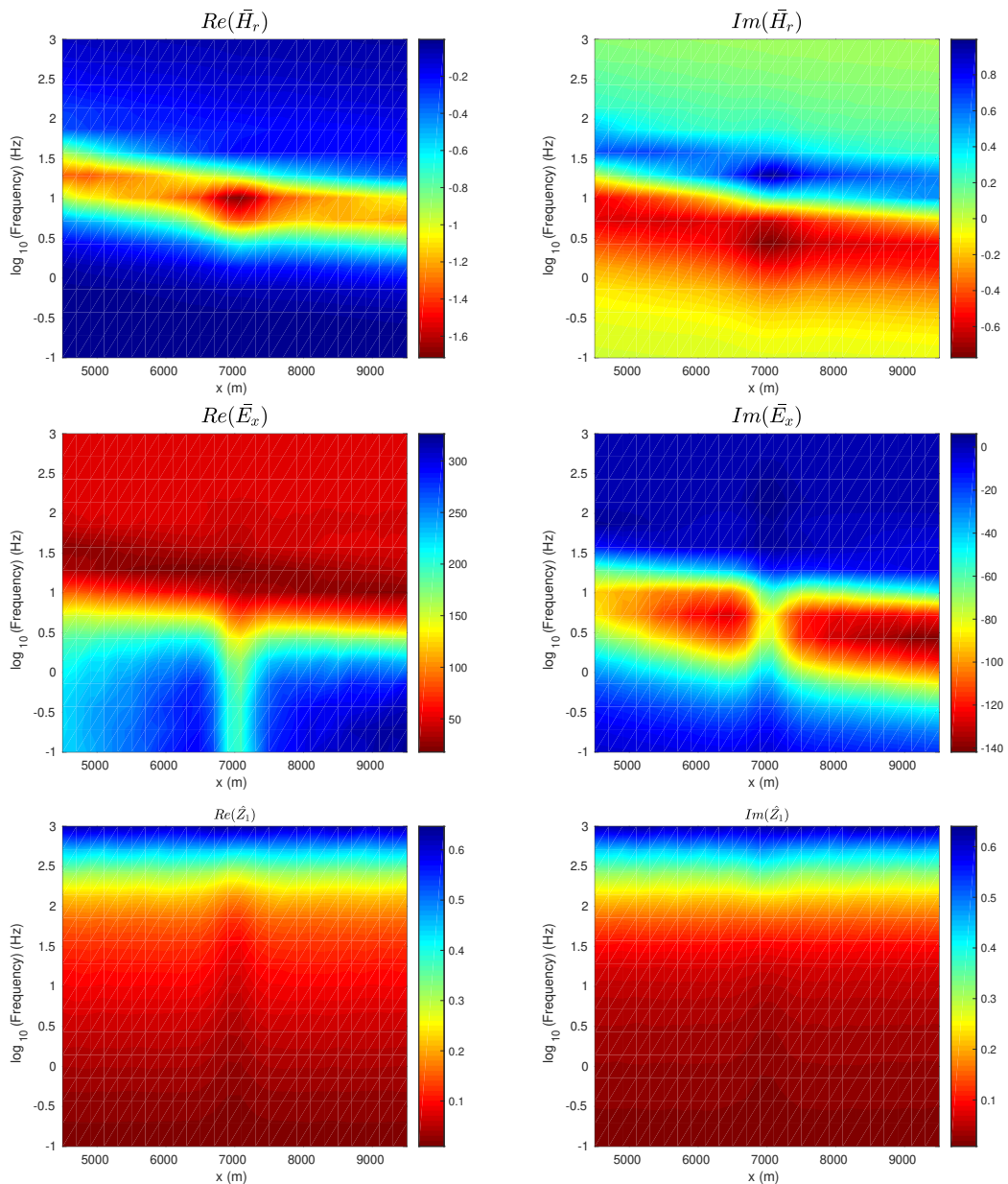


Figure 6.9: EMMF, CSAMT and MT synthetic observed data generated from Model 3.

The resistivity models obtained using the LCI technique using GS and TV regularizations are in Figures 6.10 and 6.11, respectively.

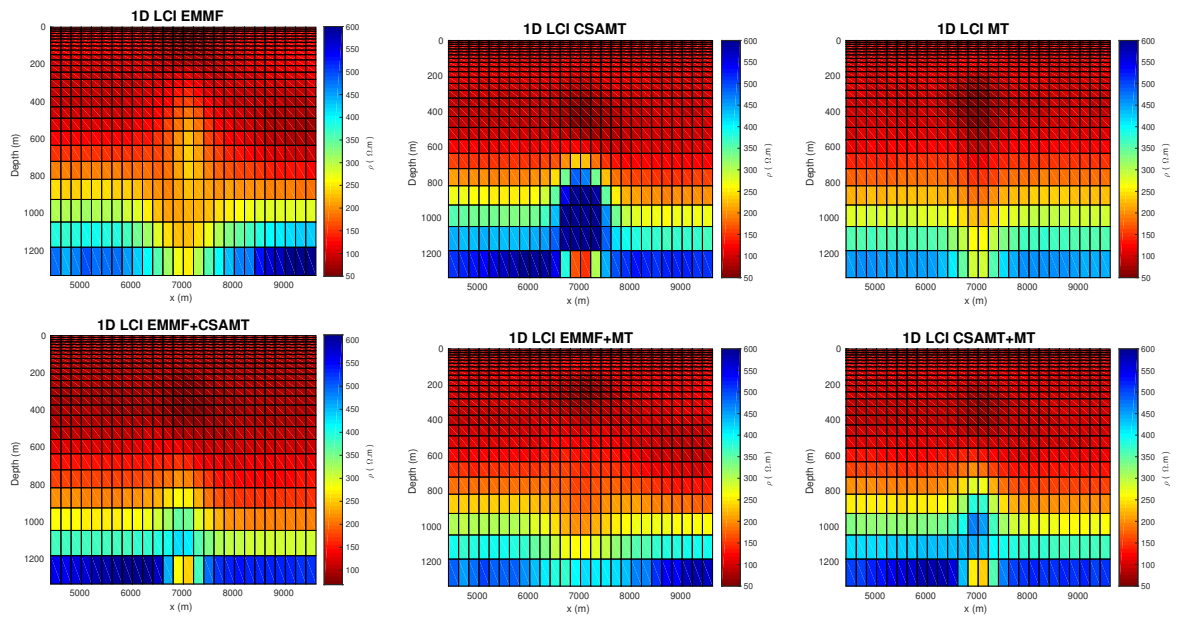


Figure 6.10: Final pseudo-2D models obtained by isolated and joint inversion of the EMMF, CSAMT and MT methods using the Global Smoothness regularization.

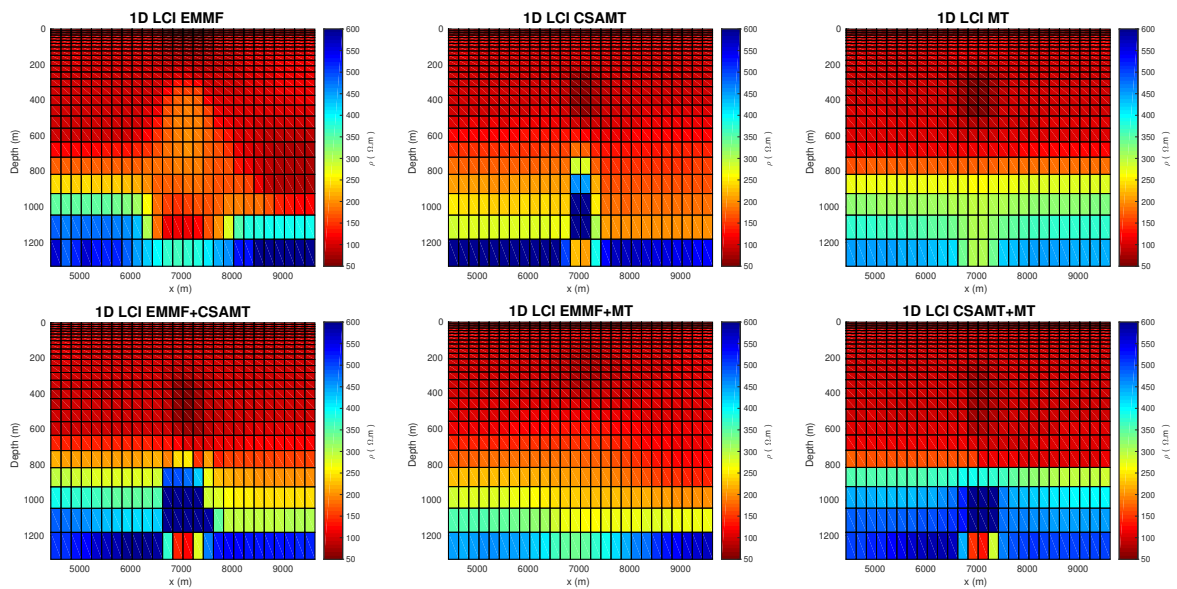


Figure 6.11: Final pseudo-2D models obtained by isolated and joint inversion of the EMMF, CSAMT and MT methods using the Total Variation regularization.

Specifically analyzing each result for **Model 3**:

- EMMF - Similar to what happened in Model 1, this result shows a resistive body instead of a conductive one. The substrate is detected at the correct depth, but its interface continuity is impaired by the effect of the heterogeneity.
- CSAMT - It identifies the 2D conductive body and the substrate. The GS imposes smoothness regardless abrupt changes in the resistivity, therefore the interface from the upper layer to the substrate is impaired. The TV result, on the other hand, responds to the abrupt changes and detects the interface but deeper than it really is.
- MT - The MT LCI result also detects the body and the substrate. As mentioned in earlier results, the effect of the lateral constraint decreases the “shade” artifact under the target so the interface between the upper layer and the substrate is relatively well detected.
- EMMF+CSAMT - This joint LCI result is a good combination: the EMMF contributed by providing the regional information (upper layer and substrate) and the CSAMT helped with the target information (2D conductive body).
- EMMF+MT - Although this result has a good estimated regional model, the target identification was impaired because of the EMMF contribution which interferes with its estimation as resistive.
- CSAMT+MT - Together with the joint EMMF+CSAMT LCI, this result confirmed those two combinations are efficient and fast techniques to image either conductive or resistive targets since complementary information is provided by each method.

7 CONCLUSIONS

The 1D and LCI results show that joint inversion of CSAMT+MT and EMMF+CSAMT, as compared to their respective individual inversions, are effective ways for delineating geoelectrical structures, since these two methods combined provide complementary information. The EMMF and MT methods respond more efficiently to conductive targets, are largely insensitive to resistive bodies and can resolve the background regional resistivity. The CSAMT method, on the other hand, responds to both resistive and conductive targets, but the results showed a poor imaging of the subsurface geology that hosts these targets.

Results from isolated inversions of MT also illustrates cases in which this method can be useful, although the LCI technique itself might have favored the MT results to better identify the 2D targets. LCI of CSAMT-only was also able to resolve the target, however in some results the host medium presented unwanted resistivity artifacts. The 1D LCI proved not to be a good alternative for inverting 2D EMMF data, since the LCI of EMMF-only presented problems in various cases, both in the attempt to resolve conductive and resistive targets. On the other hand, EMMF and MT methods played a unique role in the joint approaches contributing with the estimation of the background.

Moreover, the use of both LCI technique and analytical derivatives to calculate the Jacobian were excellent in terms of generating very fast and accurate (if compared to finite differences approach) results, resulting in an efficient and inexpensive tool for quick imaging.

REFERENCES

- Abramowitz, M., and I. A. Stegun, 1964, Handbook of mathematical functions with formulas, graphs, and mathematical tables, ninth dover printing, tenth gpo printing ed.: Dover.
- Abubakar, A., M. Li, G. Pan, J. Liu, and T. Habashy, 2011, Joint mt and csem data inversion using a multiplicative cost function approach: *Geophysics*, **76**, F203–F214.
- Auken, E., and A. V. Christiansen, 2004, Layered and laterally constrained 2d inversion of resistivity data: *Geophysics*, **69**, no. 3.
- Auken, E., A. V. Christiansen, B. H. Jacobsen, N. Foged, and K. I. Sorensen, 2005, Piecewise 1d laterally constrained inversion of resistivity data: *Geophysical Prospecting*, **53**.
- Auken, E., N. Foged, A. V. Christiansen, and K. Sørensen, 2007, Enhancing the resolution of the subsurface by joint inversion of x-and z-component skytem data: *ASEG Extended Abstracts*, **2007**, 1–4.
- Candansayar, M. E., and B. Tezkan, 2008, Two-dimensional joint inversion of radiomagnetotelluric and direct current resistivity data: *Geophysical Prospecting*, **56**, 737–749.
- Constable, S., and C. J. Weiss, 2006, Mapping thin resistors and hydrocarbons with marine em methods: Insights from 1d modeling: *Geophysics*, **71**, G43–G51.
- Constable, S. C., R. L. Parker, and C. G. Constable, 1987, Occam’s inversion: A practical algorithm for generating smooth models from electromagnetic sounding data: *The Leading Edge*, **52**, no. 3.
- Crepaldi, J. L. S., M. P. P. Buonora, and I. Figueiredo, 2011, Fast marine csem inversion in the cmp domain using analytical derivatives: *Geophysics*, **76**, no. 5.
- Dias, C., O. de Lima, H. Sato, and J. Moraes, 2006, Contribution to oil exploration and development—a successful inductive multi-frequency em survey on-shore brazil: Presented at the 68th EAGE Conference and Exhibition incorporating SPE EUROPEC 2006.
- Dias, C., O. Lima, and H. Sato, 2012, Evaluation of the multi-frequency electromagnetic method in exploration and imaging of hydrocarbon continental reservoirs: *Boletim de Geociencias da Petrobras*, **20**, 165–192.
- Dias, C., H. Sato, M. Machado, and O. Lima, 2019, Multi-frequency electromagnetic method for inductive measurement of ground ip and resistivity: *Geophysical Prospecting*, **67**, 210–225.
- Dias, C. A., 1968, A non-grounded method for measuring electrical induced polarization and conductivity: PhD thesis, University of California, Berkeley.
- , 2000, Developments in a model to describe low-frequency electrical polarization of rocks: *Geophysics*, **65**, 437–451.

- Dias, C. A., H. K. Sato, and O. A. de Lima, 2005, Multi-frequency em method for hydrocarbon detection and for monitoring fluid invasion during enhanced oil recovery, *in* SEG Technical Program Expanded Abstracts 2005: Society of Exploration Geophysicists, 602–604.
- Farias, H., 2012, Modelagem numérica de dados mcsem 2.5-d: Master's thesis, Programa de Pós-Graduação em Geofísica, Universidade Federal do Pará.
- Ismail, N., G. Schwarz, and L. B. Pedersen, 2011, Investigation of groundwater resources using controlled-source radio magnetotellurics (csrmt) in glacial deposits in heby, sweden: *Journal of Applied Geophysics*, **73**, 74–83.
- Jegen, M. D., R. W. Hobbs, P. Tarits, and A. Chave, 2009, Joint inversion of marine magnetotelluric and gravity data incorporating seismic constraints: Preliminary results of sub-basalt imaging off the faroe shelf: *Earth and Planetary Science Letters*, **282**, 47–55.
- Kang, S., S. J. Seol, Y. Chung, and H.-S. Kwon, 2013, Pitfalls of 1d inversion of small-loop electromagnetic data for detecting man-made objects: *Journal of applied geophysics*, **90**, 96–109.
- Lei, D., X.-H. Meng, P. Hu, F.-G. Zhao, and S.-M. Wang, 2010, A study on 2d csamt forward modeling and inversion with a dipole source and topography and its applications: *Chinese Journal of Geophysics*, **53**, 281–294.
- Lin, C., H. Tan, W. Wang, T. Tong, M. Peng, M. Wang, and W. Zeng, 2018, Three-dimensional inversion of csamt data in the presence of topography: *Exploration Geophysics*, **49**, 253–267.
- Machado, M. B., and C. A. Dias, 2012, Zone of main contribution to the measured signal for a circular current loop source and receiver on the surface of a conductive half-space: *Geophysical Prospecting*, **60**, 1167–1185.
- Machado, M. V. B., 2009, An analytical study and application of the multi-frequency electromagnetic method to mapping and identification of fluids in petroleum onshore reservoirs: PhD thesis, North Fluminense State University – Macaé, Brazil [in Portuguese].
- Mackie, R., M. D. Watts, and W. Rodi, 2007, Joint 3d inversion of marine csem and mt data, *in* SEG Technical Program Expanded Abstracts 2007: Society of Exploration Geophysicists, 574–578.
- Marquardt, D. W., 1963, An algorithm for least-squares estimation of non-linear parameters: *J. of the Society for Industrial and Applied Mathematics*, **11**, 431–441.
- Martins, C. M., W. A. Lima, V. C. Barbosa, and J. ao B. Silva, 2011, Total variation regularization for depth-to-basement estimate: Part 1 - mathematical details and applications: *Geophysics*, **76**, I1–I12.
- Miorelli, F., 2011, Joint laterally constrained inversion of csem and mt data: Presented at the 73rd EAGE Conference & Exhibition incorporating SPE EUROPEC 2011.

- Mitsuhata, Y., T. Uchida, and H. Amano, 2002, 2.5-d inversion of frequency-domain electromagnetic data generated by a grounded-wire source: *Geophysics*, **67**, 1753–1768.
- Pedreira, A., S. Martos-Rosillo, J. Galindo-Zaldívar, M. Rodríguez-Rodríguez, J. Benavente, J. Martín-Rodríguez, and M. Zúñiga-López, 2016, Unravelling aquifer-wetland interaction using csamt and gravity methods: the mollina-camorra aquifer and the fuente de piedra playa-lake, southern Spain: *Journal of Applied Geophysics*, **129**, 17–27.
- Perez, J. D. G., 2016, Modelagem numérica bidimensional de dados csamt com fonte dipolar elétrica usando elementos finitos: Master's thesis, Programa de Pós-Graduação em Geofísica, Universidade Federal do Pará.
- Piedade, A., 2014, Inversão 1d e 2d de dados do método eletromagnético a multi-frequência - emmf: Master's thesis, Programa de Pós-Graduação em Geofísica, Universidade Federal do Pará.
- Piedade, A., and C. Régis, 2014, Inversion of data from the multifrequency electromagnetic method—emmf, *in* SEG Technical Program Expanded Abstracts 2014: Society of Exploration Geophysicists, 808–812.
- Piedade, A., C. Regis, and C. Nunes, 2015, Equality constraints in 2d inversion of data from the electromagnetic multi-frequency method-emmf: Presented at the 77th EAGE Conference and Exhibition 2015.
- Pujol, J., 2007, The solution of nonlinear inverse problems and the Levenberg-Marquardt method: *Geophysics*, **72**, W1.
- Santos, F. A. M., 2004, 1d laterally constrained inversion of em34 profiling data: *Journal of Applied Geophysics*, **56**, no. 2.
- Sasaki, Y., 1989, Two-dimensional joint inversion of magnetotelluric and dipole-dipole resistivity data: *Geophysics*, **54**, 254–262.
- Sifontes, R. V., H. K. Sato, and Z. I. Moumoni, 2016, Relief geometric effects on frequency-domain electromagnetic data: *Geophysics*, **81**, E287–E296.
- Silva, V., 2012, Modelagem 2,5d do campos usados no método eletromagnético a multi-frequência - emmf: PhD thesis, Programa de Pós-Graduação em Geofísica, Universidade Federal do Pará.
- Tikhonov, A. N., and V. Y. Arsenin, 1977, *Solutions of ill-posed problems*: New York: Winston.
- Vogel, C. R., 1997, Nonsmooth regularization: Rundell (Eds.), *Inverse Problems in Geophysical Applications*, 1–11.
- Vozoff, K., 1991, The magnetotelluric method, *in* *Electromagnetic Methods in Applied Geophysics: Volume 2, Application, Parts A and B*: Society of Exploration Geophysicists, 641–712.
- Vozoff, K., and D. Jupp, 1975, Joint inversion of geophysical data: *Geophysical Journal International*, **42**, 977–991.

- Ward, S. H., G. W. Hohmann, and M. Nabighian, 1987, Electromagnetic theory for geophysical applications: *Electromagnetic methods in applied geophysics*, **1**, 131–311.
- Werthmüller, D., K. Key, and E. C. Slob, 2019, A tool for designing digital filters for the hankel and fourier transforms in potential, diffusive, and wavefield modeling: *Geophysics*, **84**, 1–43.
- Zonge, K. L., and L. J. Hughes, 1991, Controlled source audio-frequency magnetotellurics, *in* *Electromagnetic Methods in Applied Geophysics: Volume 2, Application, Parts A and B*: Society of Exploration Geophysicists, 713–810.